The Fluid Dynamics of Swimming Microorganisms and Cells

Ganesh Subramanian[1] and Prabhu R. Nott[2]

In this review, we describe the fluid mechanics of swimming microorganisms, with an emphasis on recent developments. We begin with the mechanics of individual swimmers, and describe the requirement for a non-reciprocal cyclic swimming stroke for net displacement in the absence of inertia. We discuss Purcell's three-link swimmer and other artificial models as simple pedagogical examples. Thereafter, we consider the swimming of real microorganisms, which may be classified into ciliates and the flagellates. In addition to the stroke kinematics, we examine the nature of the fluid velocity field around a swimmer, which governs the hydrodynamic interactions between swimmers. We then consider the large-scale hydrodynamics in a suspension of swimmers, our efforts motivated primarily by experimental observations of coherent motion. The theoretical analyses fall into two categories: the first considers coherent motion that arises from the coupling of gravity with the density difference between the swimmer and the suspending fluid. The second category is more recent, and examines the smaller-scale coherent motion, in the absence of buoyancy forces, that is driven by the anisotropic orientation distribution of the swimmer force-dipoles. We then describe a variety of discrete simulation methods, wherein the motion of every swimmer is tracked in time. The continuum theories and simulations reveal fundamental differences in the collective dynamics between suspensions of pushers, pullers and squirmers; only suspensions of pushers, for instance, are predicted to be linearly unstable. Despite the successes of the theoretical and computational methods, significant issues remain unexplained, some of which are highlighted towards the end of the review.

[1]*Engineering Mechanics Unit, Jawaharlal Nehru Centre for Advanced Scientific Research, Jakkus, Bangalore 560064, India*
sganesh@jncasr.ac.in

[2]*Department of Chemical Engineering, Indian Institute of Science, Bangalore 560 012, India*
prnott@chemeng.iisc.ernet.in

1. Introduction

The motility of living organisms is an important factor in determining their evolutionary survival. While its importance is intuitively obvious in the case of large animals—they have to go in search of food for sustenance—it is an equally pressing problem for our evolutionary ancestors, namely microscopic organisms. This is because the rate of supply of nutrients, on length scales of the order of the size of a microorganism, is controlled by molecular diffusion. While this is adequate in a nutrient-rich medium, typically each organism competes with several others in its neighborhood. Motility is thus essential to escape from the local environment and seek other more favorable regions. Motility of cells in most higher organisms too is of the essence for the survival of the species, the swimming of spermatozoa and the crawling of macrophages towards invading pathogens being two examples. This review is confined to the

swimming of microorganisms and cells in a fluid medium. We discuss the ingenious ways in which nature has evolved mechanisms for motility, and its close relation to the mechanics of the ambient fluid. We also discuss the collective motion caused by a suspension of interacting swimmers, and the interesting phenomena that result. Only a small portion of this review pertains to original work of the authors—rather it relies heavily on many previous reviews, monographs and archived research articles on the fluid dynamics of swimming microorganisms.

Carangiform locomotion refers to a propulsion mechanism in several fish species and aquatic mammals wherein thrust is generated by an oscillation of the tail with little deformation of their frontal parts.

2. Swimming at Low Reynolds Number

The size L and swimming velocity U of most swimming microorganisms are such that the Reynolds number $Re = \rho u_0 L/\eta$ is very small.[82,100,118] Here, ρ and η are the density and viscosity of the fluid medium. This means that the fluid motion is in the creeping flow regime, governed by the Stokes equations

$$-\nabla p + \eta \nabla^2 u = 0, \quad \nabla \cdot u = 0 \qquad (1)$$

where p and u are the pressure and velocity fields in the fluid, respectively. For instance, the bacterium Escherichia Coli has a length L of about 10 μm (including both head and tail, see fig. 1), and swims at a speed of about 10 μm/s; this leads to $Re \sim 10^{-4}$. In this regime, the inertia of the fluid and the swimmer play no role, and hence, propulsion does not come from bursts of acceleration generated by 'pushing' the fluid back, as in the swimming of fish and flying of birds. Indeed, the overdamped dynamics in the limit $Re \ll 1$ implies that the coasting distance on account of any momentum gained from the transient action of the propulsive element would be of the order of Angstroms! Thus, for a density-matched Stokesian swimmer, the net force and torque must always be zero, implying that the propulsive force (thrust) instantaneously balances the drag.[82,118]

E. coli is a rod-shaped bacterium (a prokaryote – single-celled organisms lacking a membrane-bound nucleus or specialized organelles) that is commonly found in the lower intestine of warm-blooded organisms. It swims by rotating a helical flagellar bundle.

An important point to be made in the context of low-Re-swimming is the absence of an obvious separation between the resistive (drag) and propulsive elements since both act via viscous stresses. In the inertial realm ($Re \gg 1$), there is often a clear separation between the two. This is exemplified, for instance, by aquatic swimmers belonging to the order percomorphi who have adopted a Carangiform mode of propulsion with the propulsive element (a large crescent-shaped tail) being well separated from the streamlined body (that contributes the primary resistance) by a narrow neck.[82] As pointed out by Taylor,[118] this must be contrasted with the low Re scenario wherein such a separation would result in sub-problems of a very different character. For instance, although the problem of a two-dimensional Stokesian swimmer is a well-posed one, a separation into thrust and drag sub-problems would lead to the well-known Stokes paradox[80] (the ability of a translating cylinder to move fluid infinitely far from it). Although not as dramatic in three dimensions, the difference between the rates of decay of the velocity field due to a particle moving under an imposed force ($u \sim O(1/r)$), and that due to a force-free swimmer ($u \sim O(1/r^2)$), nevertheless leads to enormous differences in the volume of fluid displaced.[42] This aspect has aroused interest in recent times with regard to a possible biogenic source of ocean mixing.[114]

A fundamental constraint on the stroke kinematics of Stokesian swimmers arises from the (dynamic) reversibility of the Stokes equations. Simply stated, the principle of reversibility implies that 'reversing the motion of all (rigid)[134] boundaries reverses time' This then leads to the famous Purcell scallop theorem: a scallop, a mollusk that opens and closes its shell periodically (see fig. 2), cannot swim at zero Re.[78,100] The alternate opening and closing motions lead to no net displacement over a cycle, since the asymmetry between converging and diverging flows is absent in the inertialess limit (a real scallop belongs to the inertial realm). Note that since time does not appear explicitly in the Stokes equations (1), any change in the rates of opening and closing is irrelevant. The conclusion then is that the stroke kinematics at zero Re, although cyclic, have to be non-reciprocal to result in a non-trivial stroke-averaged velocity. This in turn requires the swimmer to have at least two configurational degrees of freedom (the scallop has one).

Figure 1: A schematic of a swimming *E.Coli*. Reproduced in part from 'Collective hydrodynamics of swimming microorganisms', Koch, D.L. and Subramanian, G., Annual reviews of fluid mechanics, 2011, 43, 637-659.

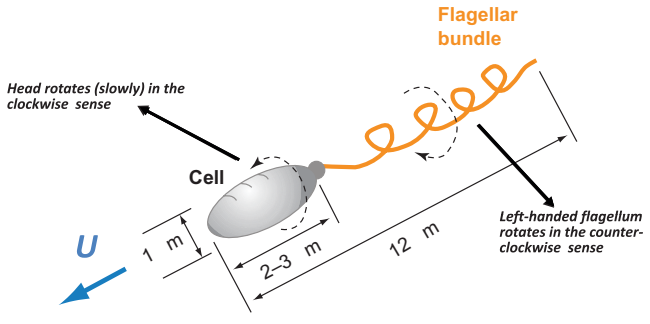

Figure 2: The reciprocal motion of a hypoethetical (two-dimensional) scallop will not lead to swimming at $Re = 0$. Although the reversible protocol depicted would appear to lead to a swimming motion with the hinge in front, for any finite Re, the actual (3D)-scallop, in fact, does the reverse; it swims with the hinge at its rear.

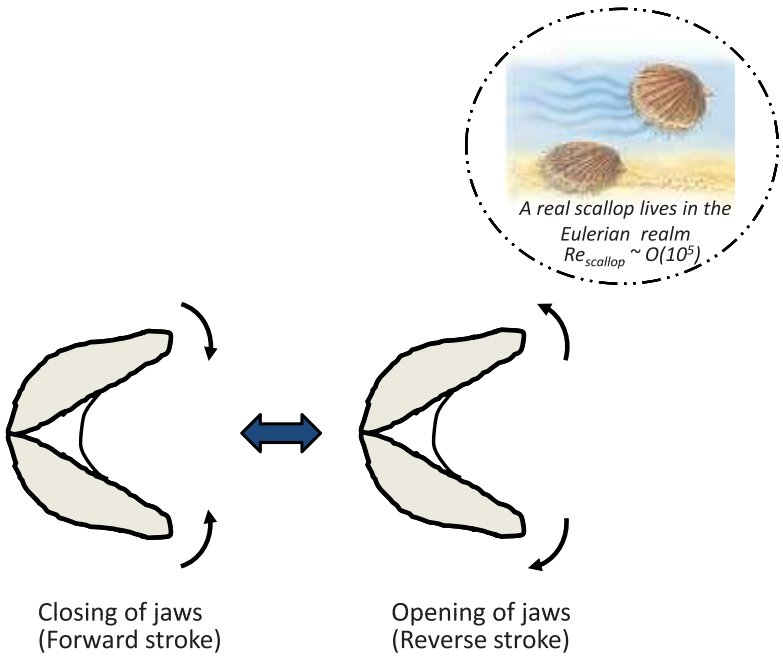

There have been many efforts at examining non-reciprocal kinematics, motivated both from a fundamental point of view[43,64,73,79,91,110] and from the desire to design simple micro-machines.[41,66,81] Herein, we only illustrate two of the simplest swimming protocols involving the minimum needed (two) degrees of freedom. The first is the so-called Purcell's swimmer (fig. 3a), originally proposed by Purcell.[79,100,117] It is a two-hinged body composed of three rigid links where the terminal links rotate alternately, and in opposite senses, relative to the middle link. The non-reciprocity leading to a net drift arises from the dependence of the swimmer resistance tensor on the relative inclinations of the links. The second is the trumbbell-swimmer (fig. 3b) proposed more recently by Najafi and Golestanian,[49,91] and wherein the non-reciprocity arises due to the differing inter-sphere spacings, and the resulting differences in hydrodynamic interactions; the trajectories of the two swimmers in the relevant configuration spaces is also shown in fig. 3 to illustrate the non-reciprocal character of the deformation. A reasonably straightforward analysis leads, in the limit of small amplitudes (and with the added assumption of slender links for Purcell's swimmer), to the following expressions for the stroke-averaged swimming velocities at leading order:

$$U_{Purcell} = \frac{11}{90}(\Omega L)\theta_0, \tag{2}$$

$$U_{trumbbell} = \frac{7}{48}\frac{U^2(aT)}{R^2}, \tag{3}$$

where Ω and U are the angular speed of the link and the translational speed of the spheres (each assumed constant) for the Purcell and Najafi-Golestanian swimmers, respectively, and T is the duration of a single stroke in the latter case; the remaining symbols are defined in figure 3. For the assumed constant velocity scenario, the calculation is just as easily extended to arbitrary stroke amplitudes; for the Najafi-Golestanian swimmer, the resulting swimming velocity is given by.[49]

$$U_{trumbbell} = \frac{U_a}{R}\left[\frac{\frac{UT}{R}}{(1-\frac{UT}{R})} + \frac{R}{2UT}\ln\left(\frac{1-\frac{UT}{R}}{(1-\frac{UT}{2R})^2}\right)\right], \tag{4}$$

with an expansion in the limit $UT/R \ll 1$ leading to (3).

While the swimming protocols described above are important from the pedagogical point of view, as will be seen in the next section, real micro-organisms have largely adopted a travelling-wave motif as the prototypical non-reciprocal deformation. The above protocols above may, in fact, be interpreted as 'sections' of a travelling wave deformation (Purcell: transverse wave, Najafi-Golestanian: longitudinal wave);[7] the swimming velocities, given by (2) and (3), are thus of the same general form as that obtained when a travelling wave deformation drives the swimming motion (see § 3). Before examining the principal modes of swimming in microorganisms, we summarize the various physical effects that lead to a breakdown of the reversibility constraints inherent in the scallop theorem. One source of irreversibility is associated with the rheology of the swimming medium—a time-reversible stroke kinematics would in general lead to a net drift in a viscoelastic medium both due to the non-linearity in the constitutive equations and the existence of an intrinsic relaxation time scale.[77] Accounting for the elastohydrodynamic coupling between the swimmer arms and the fluid medium in the original scallop model would again allow for a net drift, since the deformed arms would

Figure 3: An illustration of the non-reciprocal stroke kinematics for the (a) Purcell and (b) trumbbell swimmers. The figures illustrate the changing internal configurations in a reference frame that translates and rotates with the swimmers; as a result, the central link in the Purcell swimmer and the central sphere in the trumbbell swimmer appear stationary. The translations or rotations of the swimmer as a whole arise as a consequence of the force-free and torque-free constraints. Depiction of the changing configurations in a lab reference frame requires a detailed analysis.[79]

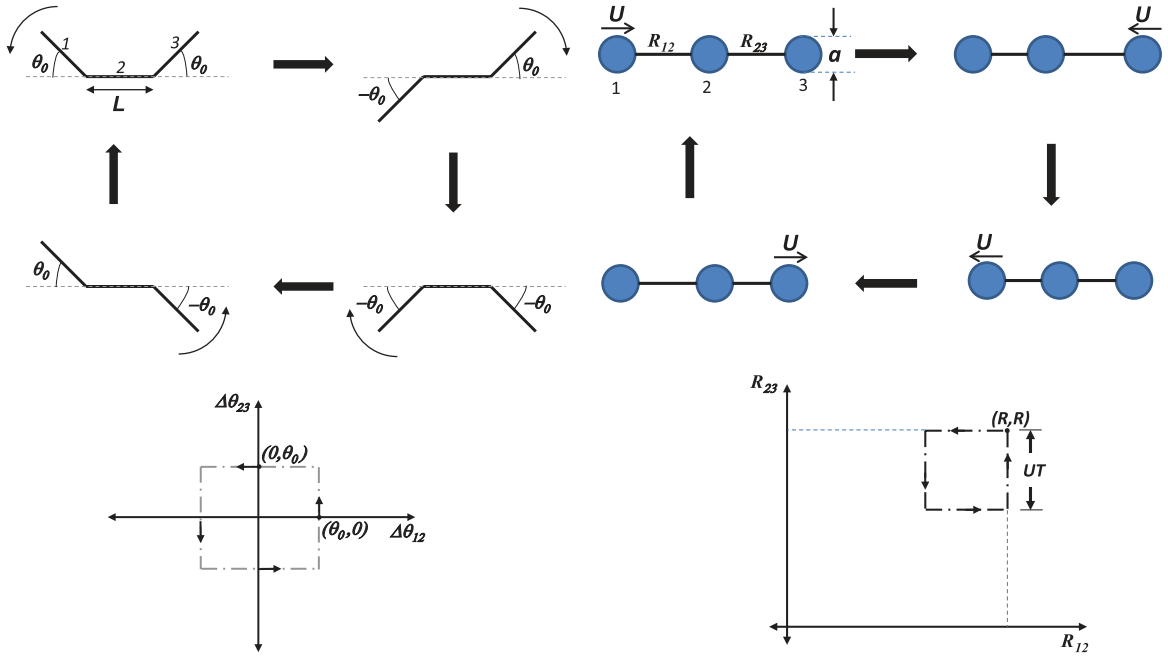

prevent an exact retracing of the configurations in the reverse stroke.[100,130] Hydrodynamic interactions provide another route to non-reciprocity (a version of which appears in the trumbbell swimmer above); thus, a collection of interacting scallops can swim if the individual reciprocal motions are suitably staggered in phase.[76]

Finally, we return to the factor that is, by definition, absent in the Stokesian realm: fluid inertia. A reciprocating scallop, on account of its inherent asymmetry in shape, will swim at any finite *Re*, albeit with a vanishingly small velocity in the limit $Re \to 0$. A more interesting scenario arises when the sequence of swimmer configurations traced during a single cycle remains fore-aft symmetric, since such a symmetry would, in principle, preclude directional motion even at finite *Re*. Childress and co-workers.[1,31,32,86] have addressed the intriguing question of a possible transition to a flapping mode of swimming, with increasing Re_f, via a symmetry-breaking bifurcation of the Navier-Stokes equations—a bifurcation that would then be the means of connecting the Stokesian and inertial realms; here, Re_f is a Reynolds number based on the flapping frequency that characterizes the reciprocating motion. The authors showed that a net translation arises as the non-linear saturated state of a finite Re_f instability of a reciprocal flapping protocol. That such a bifurcation must occur may be argued based on earlier work by Karman and Burgers who showed that a transversely oscillating plate (a fore-aft symmetric configuration at all instants) immersed in a free stream develops a thrust in the inviscid limit. Since a stationary plate ($Re_f = 0$) must exhibit a drag instead, the force on the plate must evidently vanish at a finite Re_f.[31] Evidence for the onset of a flapping mode beyond a critical Re_f has been found for *Clione antarctica*, a mollusc capable of both a non-reciprocal ciliary mode of propulsion (at lower speeds and a reciprocal flapping motion at higher ones).[32] It is worth noting that although the appearance of swimming via a bifurcation requires the complete absence of any spatial asymmetry, the phenomenon continues to be relevant in the presence of such asymmetries (as for the scallop above) when there would be a net swimming motion at any finite Re_f (a continous breakdown of the scallop theorem, so to speak).[75] The existence of an underlying bifurcation should manifest as a rather abrupt increase, at an $O(1)$ value of Re_f, from a small value proportional to any spatial asymmetry to an $O(1)$ value related to the

non-linear interaction between the reciprocating swimmer and the shed vorticity.

3. The Motion of Individual Organisms and Cells

As mentioned in the earlier section, microorganisms have circumvented reversibility constraints by largely adopting a travelling wave motif. Swimming occurs due to rotating or waving thin filaments called flagella and cilia, though there are several exceptions.[135] Based on a hydrodynamical point of view (the stroke kinematics, nature of the surface deformations, hydrodynamic interactions between individual filaments etc.), the swimming mechanisms may be conveniently classified into flagellar and ciliary propulsion.[30] In the former case, swimmers exploit the motion of one or a small number of filaments on the cell; ciliary propulsion, in contrast, occurs by virtue of the non-reciprocal motion of a large number of such filaments (an interacting array that often completely covers the swimmer surface). With a few interesting exceptions,[136] ciliary propulsion is confined to the larger eukaryotes (eg. *Opalina, Paramoecium*). The smaller eukaryotes, for instance, the *Spermatozoa* and the algal species *Chlamydomonas* and typical prokaryotes (bacteria such as *Escherichia Coli, Salmonella typhimurium, Bacillus subtilis*) exhibit a flagellar swimming mode. The swimming velocity resulting from a travelling wave deformation has the general form $U \sim c(A/\lambda)^2$, in the limit of small amplitudes, where c is the wave speed and A and λ are, respectively, the wave amplitude and wavelength.[30] From (2) and (3), the swimming speeds of the Purcell and Najafi-Golestanian swimmers are seen to be of the same general form: $U_{Purcell} \sim (L/T)\theta_0^2$, $U_{trumbell} \sim (a/R)(R/T)(U_sT)^2$ where U_sT and θ_0 are a measure of the linear and angular amplitudes; the additional factor of $O(a/R)$ in $U_{trumbbeli}$ reflects the strength of the hydrodynamic interactions that make the configuration changes non-reciprocal.

From the point of view of ultrastructure and physiology, the eukaryotic cilium and flagellum are virtually identical (the cilia tend to be shorter than flagella, but this distinction is superficial), and differ profoundly from the prokaryotic (bacterial) flagellum. The latter is a hollow helical filament,[137] about 20 nm in diameter and composed of the protein flagellin, that generates propulsion by rotating about its axis. This rotation (at a typical frequency of $O(50\ Hz)$) is accomplished by a remarkable motor-stator apparatus at the base of the head (see fig. 4) powered by the flow of H^+ or Na^+ ions through ion channels at the base of the flagellum. Cilia (and eukaryotic flagella) are much thicker, about 200 nm in diameter, and have a more intricate protein structure. As shown in fig. 5, a configuration called the axoneme, composed of nine microtubule doublets arranged in a circle around a central pair, is enclosed by an extension of the cell membrane, and swimming occurs by the propagation of bending waves, planar or helical, from head to filament-tip. Unlike the prokaryotic flagellum, the cilium is not a passive structure and relies on a distributed actuating mechanism wherein an elastic bending wave is caused by ATP-driven dynein motors that force the (inextensible) tubules to slide relative to each other (interestingly, Machin (1958), from the observed beating patterns of sperm flagella, whose amplitude increases from head to tail, had already concluded that the driving mechanism cannot be localized at the head, but must instead be distributed along the flagellum). It needs to be emphasized that the rotary joint in a bacterium allows for a *relative* rotation of the flagellum and the head; the head and tail must then rotate in opposite senses (the head with a smaller angular velocity on account of its larger resistance) in order to conform to a torque-free constraint. On the other hand, the tail in a flagellated Eukaryote is rigidly attached at the base of the head; any rotation of the cross-section about the local centerline (during helical wave propagation) can only occur due to head-rotation in the same sense. The basic mechanism of flagellar propulsion relies on the drag anisotropy of an elongated body. The original resistive-force theory of Gray and Hancock (1955) predicts the swimming speed of a flagellated swimmer to be proportional to $(\frac{\zeta_{\|}}{\zeta_{\perp}} - 1)$, where $\zeta_{\|}$ and $\zeta_{\perp}$ are, respectively, the local resistance coefficients for transverse and longitudinal translation. When the wavelength or pitch characterizing the flagellar motion greatly exceeds the the flagellum radius, the local motion may be regarded, at leading order, as that of a long cylinder with an identical cross-section. Viscous slender body theory yields $\zeta_{\perp} = 2\zeta_{\|} + O(\ln \kappa)^{-1}$ for a fiber of an arbitrary cross-section, $\kappa \gg 1$ being the fiber aspect ratio.[3,35] Figure 6 shows how a net translation arises, due to a rotating helical flagellum, as the cumulative drift of differential elements (each equivalent to an inclined slender fiber with the longitudinal and transverse directions being defined with respect to the local flagellum axis) in a direction transverse to the imposed rotation. Evidently, when $\zeta_{\perp} > \zeta_{\|}$, the direction of swimming is opposite to that of wave propagation. It is often the case that the helical propeller is not just a single flagellum, but instead a bundle of many. The swimming motion of

Eukaryotic cells are evolutionarily more advanced than prokaryotes, having a membrane-bound nucleus (that holds the genetic material) and other specialized membrane-bound organelles.

Figure 4: The bacterial flagellum: the left-hand-side figure is a schematic of all the parts of the flagellum; the prefix *Fl* denotes proteins associated with the flagellum, while *Mot* denotes an association with the basal motor. The right-hand-side figure is an (rotationally averaged) electron micrograph of the basal body, comprising the stator, rotor, rings and the hook.[12] Reproduced from 'Motile behavior of bacteria', Berg, H.C., Physics Today, 2000, 53, 24-29.

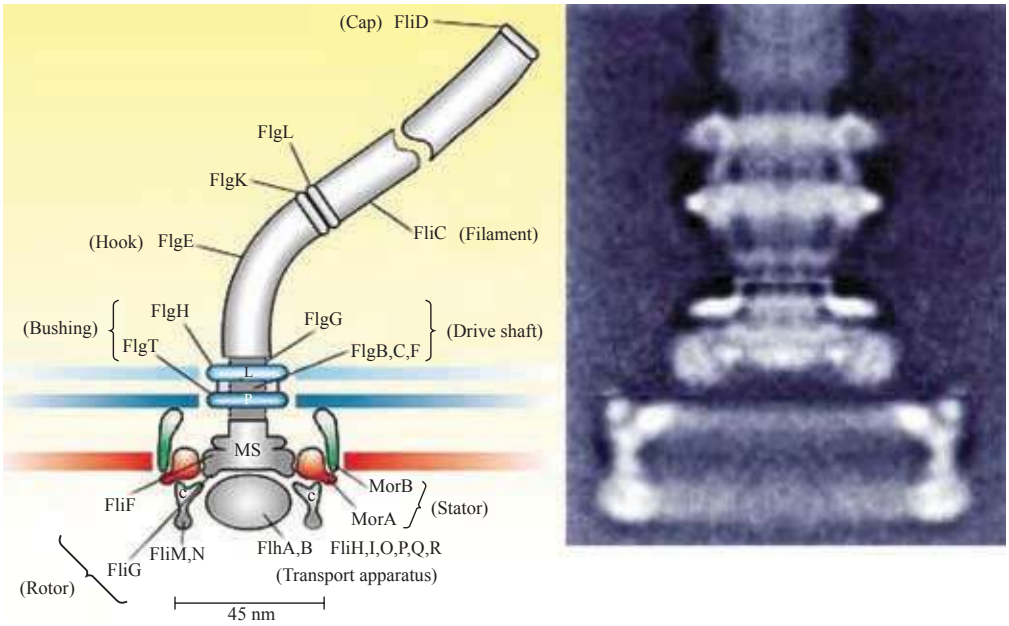

Figure 5: The structure of the eukaryotic flagellum; see text for explanation.

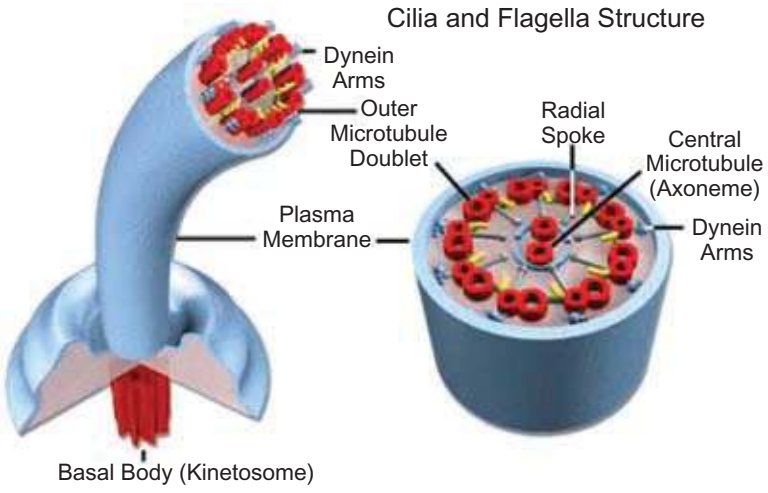

peritrichously flagellated bacteria (i.e., bacteria with several flagella projecting in different directions) such as *E.Coli*, the species most often used in experiments that demonstrate collective motion in microorganism suspensions, is driven by a rotating (helical) bundle. In *E.Coli*, the basal motor driving the flagellum can rotate both ways. For counterclockwise rotation (as viewed from the flagellum tip), the individual (left-handed) flagella come together[138] and interactions, both

Figure 6: The top figure shows why an inclined fiber, on account of the drag anisotropy, translates along a direction intermediate between its own orientation and that of the applied force (for instance, gravity). For a swimming bacterium, the imposed force distribution arises from the axial rotation of the helical flagellum, and the bottom figure shows how the induced velocities always point in the same direction.

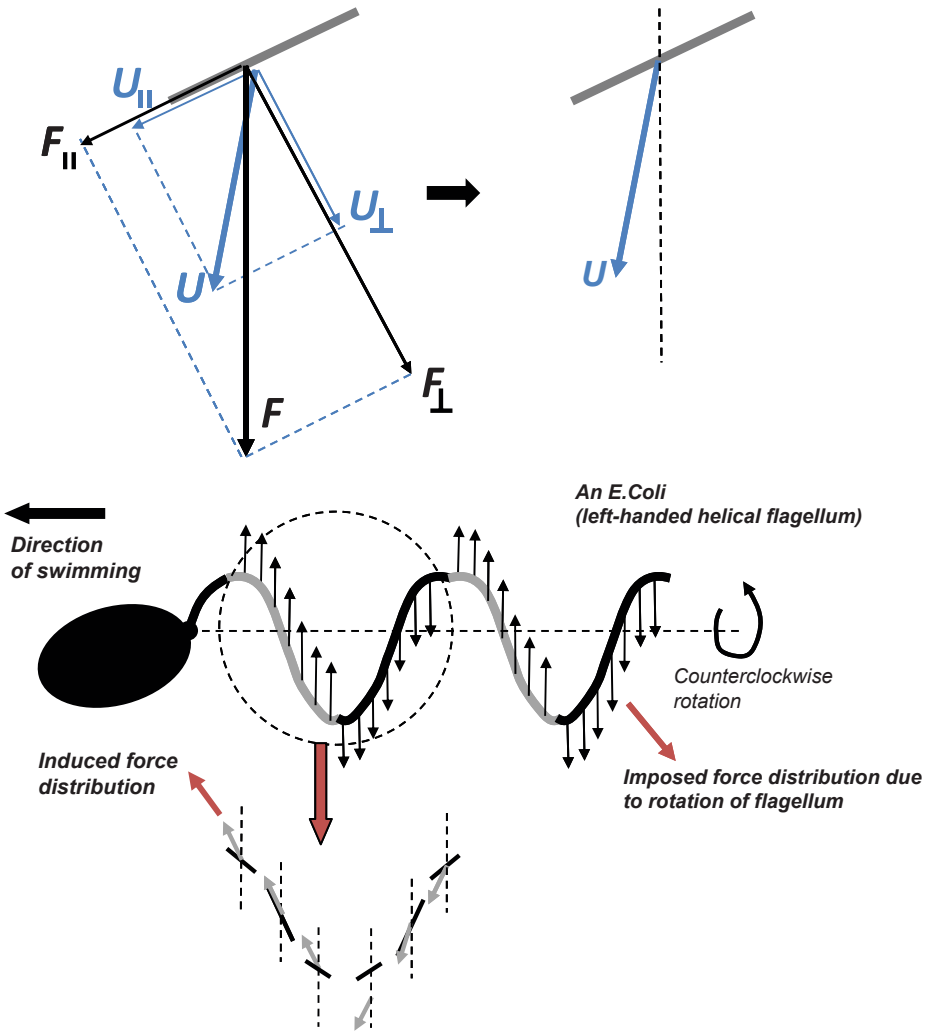

hydrodynamic and elastic, eventually drive them towards forming a single bundle.[71,105] The rotation of the bundle causes the bacterium to swim, on average, in a given direction—this is referred to as a *run*. Runs are not perfectly straight and the orientation fluctuations during a run resemble a rotary diffusion process. The motors intermittently change from a counterclock-wise to a clockwise rotation. A reversal of any one motor causes the individual flagella to come apart, causing the cell to rotate erratically—this is called a *tumble*. Resumption of the counterclockwise mode drives the bundling process in a different orientation, and the cell sets off on an another run in a different direction that is (weakly) positively correlated to the original run;[11] see fig. 7. Such a run-and-tumble motion effectively leads to the bacterium executing a random walk in three dimensions; the phenomenon of *chemotaxis* (see boxed description on page 13), results from a concentration-dependent modulation of the random walk parameters. For long times and in the absence of chemotaxis, the motion is purely diffusive, and for weakly correlated runs, the diffusivity is given by $D = \frac{U^2}{6(\frac{1}{2r} + D_r)}$ where U is the (average) swimming speed, τ is the mean-interval

Figure 7: A schematic of the run-and-tumble dynamics typically exhibited by peritrichously flagellated bacteria; the parameters given here correspond to *E.Coli*.

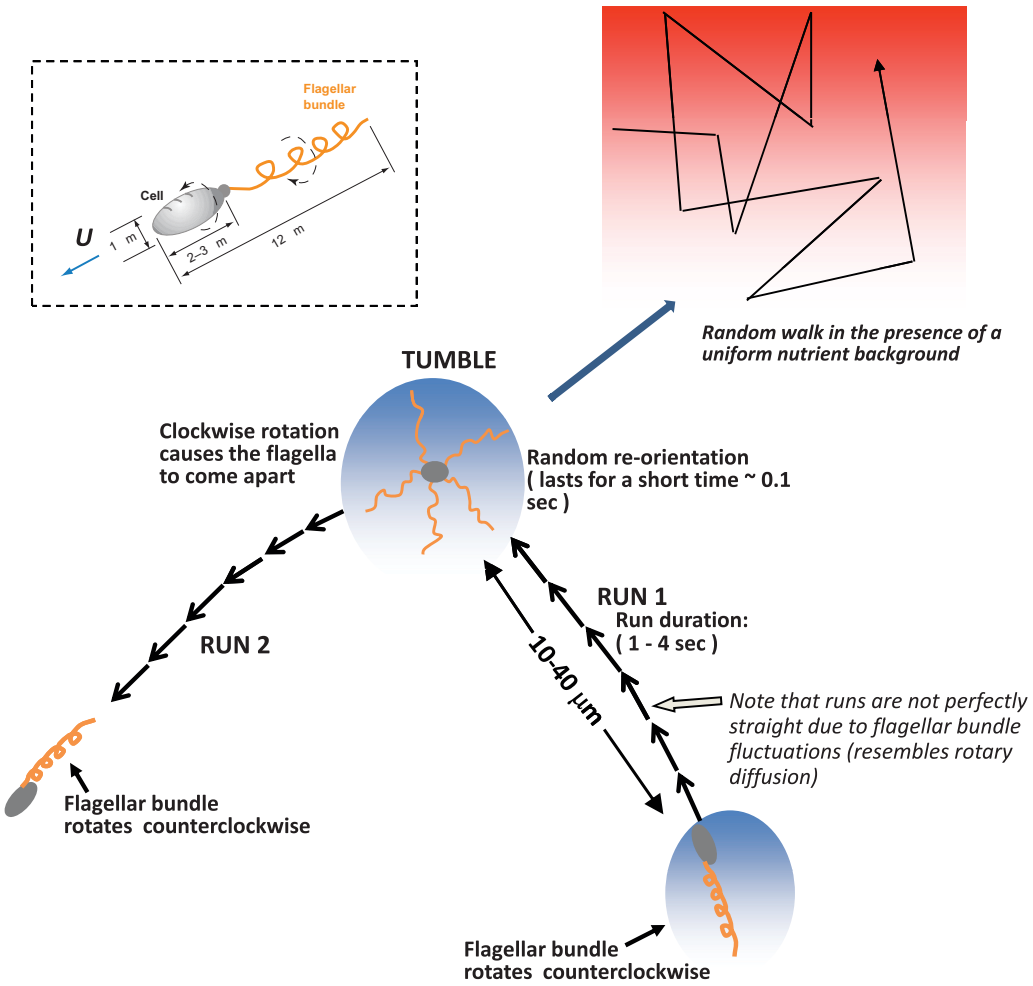

between tumbles and D_r is the rotary diffusivity characterizing the small-amplitude orientation fluctuations during a run.

The rotating helical flagellum of a bacterium drives fluid motion in a direction opposite to swimming while the head drags fluid along in the same direction. On sufficiently large length scales, the velocity field induced by a swimming bacterium like an *E.Coli* appears therefore as that due to a force-dipole with forces directed outward along the swimming axis (see fig. 8). Such swimmers are termed 'pushers'. Eukaryotes such as spermatozoa that swim by propagating an elastic bending wave from head to tail-tip are again pushers. There are organisms which exhibit the reverse anisotropy ($\zeta_\perp < \zeta_\parallel$) too, in which case the swimming occurs in the direction of wave propagation. Eukaryotes such as *Ochromonas* have a flagellum with transverse rigid projections called mastigonemes that enhance the resistance to longitudinal motion relative to a transverse one (the longitudinal motion of the flagellum would imply a transverse one for the mastigonemes). Such swimmers would again act as force-dipoles on large scales, but with the forces directed inward, and are termed 'pullers'. Another example of a puller is the algae *Chlamydomonas*, referred to above and often used in the early experiments on bioconvection,[68,70] that swims via the non-reciprocating breaststroke-like motion of a pair of anterior flagella (see fig. 9); the nature of the flagellar beat is similar to that of individual cilia to be discussed next.[139] It is worth noting that the dependence of a net translation on the drag anisotropy associated with a local motion of a two-dimensional character is not exclusive to the Stokesian realm. The local character of the resistance coefficients can be extended to higher *Re*

Figure 8: A bacterium like an *E.Coli* acts as a pusher on large length scales. Reproduced in part from 'Collective hydrodynamics of swimming microorganisms', Koch, D.L. and Subramanian, G., Annual reviews of fluid mechanics, 2011, 43, 637-659.

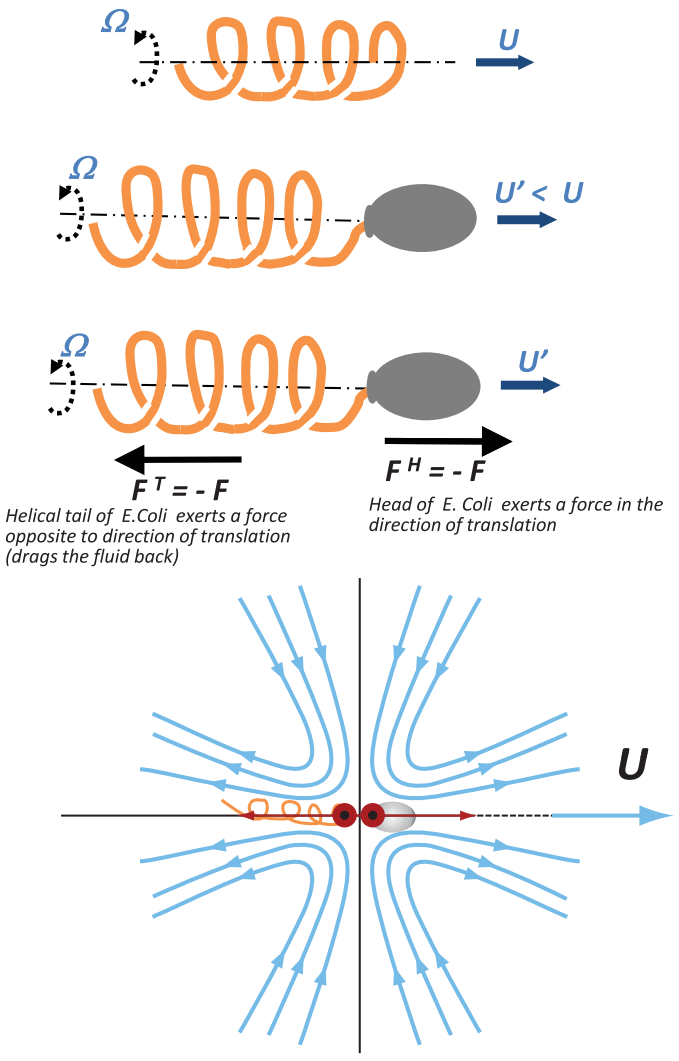

in the limit that the wavelength of the undulatory swimming mode greatly exceeds the swimmer's transverse dimensions, as was originally done by Taylor (1952); the linear scaling with the ambient velocity, of course, no longer holds at non-zero *Re*. Interestingly enough, even examples of a reversed anisotropy (again due to transverse appendages) exist in the inertial realm; polychates worms, for instance, swim by way of a 'reverse' undulatory mode.[84]

As the name suggests, the swimming motion of ciliates is driven by the polarized beats of individual cilia. The beat is similar to the one in Chlamydomonas (fig. 9) in that there is an effective stroke primarily responsible for a net displacement and then a recovery stroke where the cilium retreats to its initial position in a 'low' resistance mode. The drag anisotropy is again exploited here since the motion during the effective stroke is largely normal to the cilium axis, while that during recovery is mostly tangential (see fig. 10). In many cases, recovery may happen out of the plane of the effective stroke, leading to a three-dimensional beat. Furthermore, non-trivial phase differences between the beats of neighboring cilia often result in the propagation of metachronal waves (the travelling wave thus occurs as a secondary motif in ciliates). The direction of wave propagation may have almost any orientation relative to the plane of the effective stroke. When the wave propagation and the effective stroke are in the same direction, one refers to it as symplectic metachronism; if they are in opposite directions, one has antiplectic metachronism. If the directions are normal to one another, it is termed diaplectic; either dexioplectic or laeoplectic depending on whether the sense of rotation in going from the metachronal wave direction to the stroke direction is clockwise or anticlockwise. *Opalina* and *Paramecia* are examples of ciliated protozoa that exhibit symplectic and dexioplectic metachronism, respectively.[24]

The simplest theoretical investigation of ciliary propulsion was Taylor's original analysis[118] of the swimming of a (transversely) oscillating infinite sheet; the analysis has since been generalized to include both transverse and longitudinal degrees of freedom,[23,124] and extended to a cylindrical geometry.[17] A similar analysis for finite-sized (spherical) objects was initiated by Lighthill[83] and later extended by Blake.[18] Such analyses come under the category of envelope models where the detailed swimming microstructure (cilia) is not explicitly accounted for. Instead, the collective motion of the cilia is modelled by an impenetrable wavy surface. This is a reasonable approximation only for symplectic metachronism where the cilia tips stay close together through the entire stroke cycle. A second category, complementary to the first in the sense of attempting to account for the detailed cilia dynamics, comprises the sublayer models first proposed by Blake (1972). Herein, each cilium is modelled using slender body theory,[3] and accordingly represented as a superposition of fundamental Stokes singularities along its centerline (a valid approximation since the typical inter-cilia spacing of $O(0.3–3\ \mu m)$ is greater than the cilium diameter of $O(0.1\ \mu m)$); the dynamics of the moving centerline are prescribed apriori, and depend on the particular form of metachronism.

Figure 9: The algae, *Chlamydomonas nivalis* acts (in the stroke-averaged sense) as a puller on large length scales.

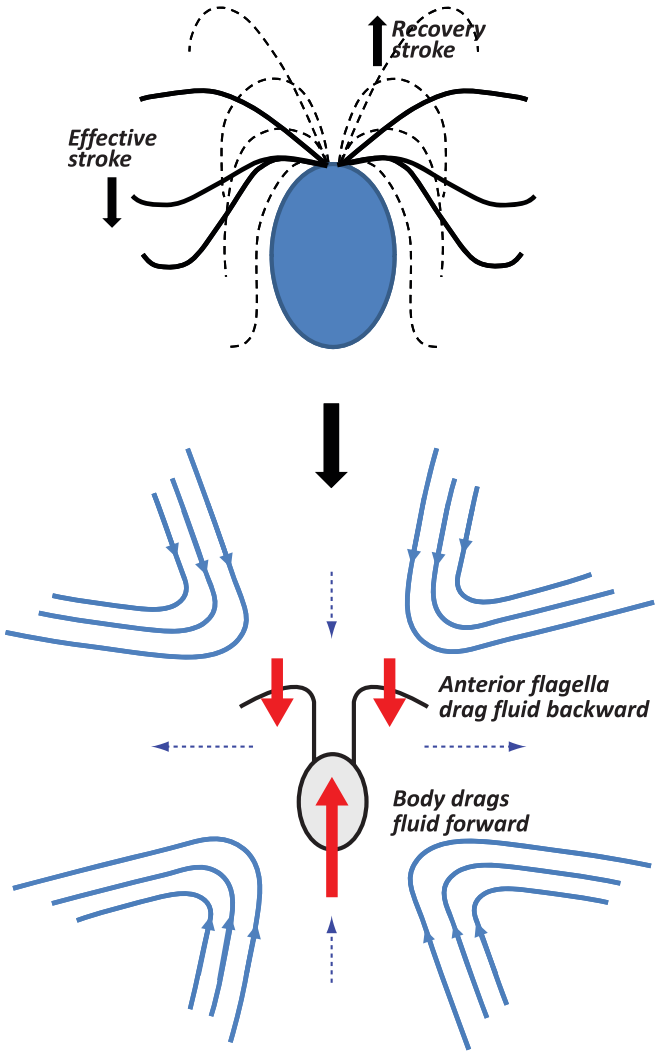

A force-dipole is formed by placing two point forces of equal magnitude but opposite direction separated by a small distance. The magnitude of the dipole is the force multiplied by the separation.

The flow in the cilia sublayer is then determined by summing the individual cilium velocity fields (in the infinite plane approximation), where the strengths of the singularities that drive the individual velocity fields are determined in a self-consistent manner from the time-and-space averaged relative velocity evaluated along a cilium. There has been a later attempt to 'patch up' the envelope and sublayer solutions in order to obtain the complete velocity field around a finite-sized swimmer.[18] Brennen (1974, 1975) has, however, rigorously analyzed the problem of a finite-sized swimmer, in the limit that the relevant length scales—the inter-cilia spacing, the metachronal wavelength (see top right of fig. 10) and the size of the organism—are well separated, via the method of matched asymptotic expansions. It is shown then that the flow around a ciliate consists of two parts: an inner solution, determined by either an envelope or a sublayer model and that describes the oscillatory flow induced by the cilia in a thin boundary layer as a function of the (slowly varying) metachronal wave parameters; and an outer steady Stokes flow solution on length scales of the order of the organism size.

In the Lighthill-Blake envelope model above, we note that although the original analysis allowed for an arbitrary surface velocity profile, the simplest most intuitive case is where the deformations of the swimmer surface are purely tangential, and further, the surface velocity variation is axisymmetric and characterized by a single spherical harmonic (the first Legendre polynomial). The resulting 'spherical squirmer' acts as a force-quadrupole on large length scales (see fig. 10 and §4). The Lighthill-Blake squirmer model has been used in recent times by Pedley and co-workers[60–63] to examine both pair-hydrodynamic interactions and large-scale collective motion in suspensions of squirmers. The version of the original (general) model used in these studies has a purely tangential surface slip induced by a combination of quadrupole and dipole singularities (at the squirmer's center). For sufficiently large magnitudes of the dipole contribution, the surface velocity reverses sign leading to a region of recirculating streamlines in the bulk. As expected, and pointed out in sections 5 and 6, the results obtained with regard to pair-trajectories,[63] diffusion,[61] rheology[60] and mass transfer (nutrient uptake; see[87]) remain sensitive to the ratio of the quadrupole and dipole coefficients. The physics leading to a reversal in the squirmer surface velocity, in a stroke-averaged scenario, and its relevance to real ciliates, appears unclear. The surface slip velocity for a swimming *Paramoecium caudatum* (a slender spheroid with an aspect ratio of about 3) has been measured using particle imagine velocimetry, and exhibits a slight fore-aft asymmetry without any reversal in direction.[59]

4. Fluid Motion Due to Individual Swimmers

Keeping in mind later sections that deal with numerical simulations and continuum theories of swimmer suspensions, we highlight the key features associated with an individual swimmer that underly such efforts. As stated above, on sufficiently large length scales, a flagellated Stokesian swimmer appears as a force-dipole; a passive particle driven by an external field such as gravity acts as a point force instead. Both

Figure 10: Ciliated eukaryotes are expected to act as force-quadrupole singularities on large scales. Reproduced in part from 'Fluid mechanics of propulsion by cilia and flagella', Brennen, C. and Winet, H., Annual reviews of fluid mechanics, 1977, 9, 339-398.

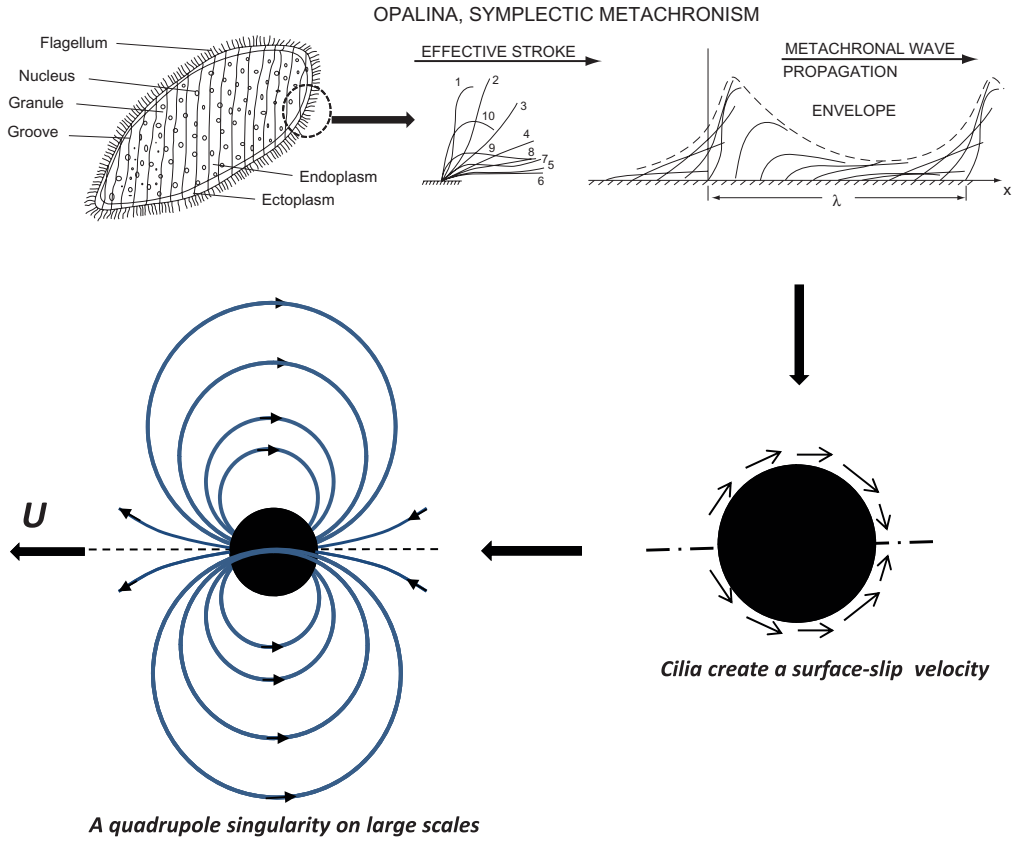

point-force ($O(1/r)$) and force-dipole ($O(1/r^2)$) velocity fields lead to long-ranged *hydrodynamic* interactions. The latter interactions have been shown to destabilize a quiescent suspension of neutrally buoyant Stokesian swimmers (see § 5). Results based on far-field interactions may be argued to have a universal character, being independent of the details of the swimming mechanism. Short-ranged interactions between swimmers, that dominate at higher concentrations, are likely to be more complicated, however. The velocity field on scales comparable to the swimmer size will be sensitive to the unsteady nature of the stroke kinematics, and thus, differ from one species to another. Recent experiments by Guasto *et al.* (2010) have used particle image velocimetry on confined films of *Chlamydomonas reinhardtii* (which swims in a manner similar to *C. Nivalis* above), and found that, while the time-averaged velocity field decays as $O(1/r)$ in the far-field (corresponding to a two-dimensional stresslet), and is consistent with that induced by the force-dipole of a puller, it also has a richer structure (including an anterior stagnation point) on scales comparable to the swimmer size; this is consistent with other independent time-averaged measurements.[40] Further, measurements of the instantaneous velocity field show that deviations from a stroke-averaged picture are quite close to the swimmer, and include the onset of flow-reversal during the recovery stroke. Theoretical analyses of pair-hydrodynamic interactions of model Stokesian swimmers[99] have, in fact, shown that the nature of pair-trajectories (attractive, repulsive, oscillatory) depend crucially on the relative phases of the swimmer stroke cycles; the phase differences between the swimmer strokes manifest as contributions that are higher-order in relation to the force-dipole.

As noted in §3, the simplest model ciliate, a 'spherical squirmer', induces an $O(1/r^3)$ disturbance field (equivalent to a degenerate Stokes quadrupole); an identical flow field is encountered in the phoretic migration of charged

The Debye layer is a measure of the thickness of the layer of counter-ions that preferentially surround a charged particle dispersed in an electrolyte solution. This cloud of counter-ions acts to screen the electric field due to the (particle) surface charge.

Marangoni effects refer to flow phenomena arising from a variation in the interfacial tension. An interface, with a varying tension, supports a jump in the tangential stresses. The pattern formation seen in the cooking pan is often driven primarily by Marangoni effects (Benard-Marangoni convection); the temperature inhomogeneities at the free surface, due to bottom-heating, lead to corresponding variations in surface tension that support convective cells.

passive spheres, under an applied electric field, in the limit of a vanishingly thin Debye layer;[2,107] drops migrating as a result of Marangoni effects, due to an imposed temperature gradient, induce a similar velocity field.[80] The $O(1/r^3)$ disturbance field is weaker than the $O(1/r^2)$ force-dipole field induced by a model flagellate. It may, in fact, be shown that a swimmer whose stroke kinematics remain invariant under a combination of time-reversal ($t \leftrightarrow -t$) and parity transformations ($\mathrm{r} \leftrightarrow -\mathrm{r}$) will act as a force-quadrupole singularity, rather than a force-dipole, on large length scales.[99] The Purcell and Najafi-Golestanian swimmers, discussed in §3, belong to this category for the case where the stroke amplitudes remain identical for the individual swimmer elements. The issue of an $O(1/r^2)$ versus an $O(1/r^3)$ velocity disturbance in the far-field is expected to be crucial with regard to the nature of the resulting hydrodynamic interactions.

Just as a swimmer causes motion of the fluid around it, it is also influenced by the fluid motion induced by other means. Apart from being advected by the local flow, the most important influence is on the swimmer orientation; since this determines the swimming direction, as also the contribution of the intrinsic force-dipoles to the bulk stress (see §5). Theoretical models of swimmer suspensions assume an active swimmer to orient, in response to an ambient shearing flow, in the same manner as a passive particle. A spherical swimmer is then expected to spin at a constant rate about the ambient vorticity axis. However, most bacteria are elongated and are expected to respond to both the ambient rate of strain and vorticity. For a passive axisymmetric particle, the orientation dynamics in an ambient linear flow is governed by the equation:

$$\dot{\mathrm{p}} = \boldsymbol{\Omega} \cdot \mathrm{p} + \mathcal{F}(\kappa)[\mathrm{E} \cdot \mathrm{p} - \mathrm{p}(\mathrm{E} : \mathrm{pp})], \qquad (5)$$

where $\mathcal{F}$ is a function of the particle aspect ratio;[72] for a spheroidal geometry, $\mathcal{F} = \frac{K^2-1}{K^2+1}$. According to (5), axisymmetric particles move along closed orbits (Jeffery orbits)[65] in simple shear flow. In the limit of large aspect ratios, a passive particle remains nearly aligned with the flow axis for an extended period of time; there are intermittent rapid flips (lasting only for a fraction $O(\kappa^{-1})$ of the orbit period) between (nearly) aligned orientations. There is, as yet, little evidence for the orientation dynamics of individual prokaryotes. Recent experiments with *Chlamydomonas reinhardtii*[101] have, however, shown significant differences between the orientation dynamics of active (live cells) and passive particles (dead cells). While the latter tumble at almost a constant rate corresponding to a nearly spherical particle, the former seem to actively resist the flow; such a resistance, likely mediated by the moving flagella, leads to an increased effiective viscosity at the same concentration (presumably due to both an intrinsic stresslet and an additional 'spin' contribution to the bulk stress).

4.1. *Chemotaxis*

In §3, we had described the run-and-tumble dynamics of peritrichously flagellated bacteria such as *E.Coli*. Of particular interest is the manner in which the parameters of this stochastic motion are modified in response to a changing chemical environment to enable the bacterium to move towards nutrient-rich regions (positive chemotaxis), or move away from toxic chemicals (negative chemotaxis). In a homogeneous environment, the statistics of the run-and-tumble motion are well approximated by a Poisson process, so that the probability of occurrence of exactly κ tumbles in a time t is $P(\kappa) = \frac{e^{-\frac{t}{\tau 0}}(t/\tau 0)^k}{k!}$. In particular, the interval between successive tumbles is exponentially distributed with a mean τ_0; for *E.Coli*, $\tau_0 \sim O(1s)$. The actual tumbling events have a much shorter duration (about $0.1s$), and may be regarded as instantaneous. As discussed in §5 (see equation (13)), a tumbling event may then be entirely characterized by a transition probability density, $K(\mathbf{p}|\mathbf{p}')$, where $\mathbf{p}$ and $\mathbf{p}'$ denote the pre- and post-tumble orientations. Perfectly random tumbles correspond to an isotropic transition probability ($K(\mathbf{p}|\mathbf{p}') = 1/(4\pi)$) and a mean-angle between successive runs of 90 degrees ($\langle \mathbf{p} \cdot \mathbf{p}' \rangle = 0$); the tumbles in *E.Coli* have a weak forward correlation with the mean re-orientation accompanying a tumble being about 68 degrees.[11]

An environment rendered heterogeneous by the gradient of a chemical (referred to as a chemo-attractant or a chemo-repellent) engenders a tactic response in the bacterium. The response is bi-phasic; that is, pronouncedly asymmetric for small chemical gradients, the asymmetry arising from a difference in threshold for increasing and decreasing attractant concentrations.[19] The runs are extended when the bacterium heads up the gradient, while remaining almost unchanged when it happens to swim the other way.[27] The previously constant mean-free time is now a function of the orientation of the bacterium trajectory (p) relative to the attractant gradient ($\zeta \mathbf{g}$), and may be generally written as $\tau = \tau_0 + F(\zeta \mathrm{g} \cdot \mathrm{p})[1 - \mathcal{H}(\mathbf{g} \cdot \mathbf{p})]$ with $F > 0$; $\mathcal{H}(z)$ here is the Heaviside function.[114] The anisotropic response results, on average, in the bacterium migrating towards attractant-

rich regions (a chemo-repellent has the opposite effect). Note that the other parameters of the run-and-tumble motion, for instance, the transition probability characterizing the tumble events, remain virtually unaltered. In this sense, *E.Coli* and other similar bacteria do not perform true chemotaxis since their swimming motion is not directly correlated to the direction of the chemical gradient. Indeed, the stochastic nature of the biased response implies that the chemotactic drift velocity is only about 10% of the bacterial swimming speed.[128] This must be contrasted with typical eukaryotes that actively steer towards favorable regions by modulating their angular velocity components (leading to a modulation of the axis of helical motion); a mechanism known as helical klinotaxis.[36,37] In both cases, however, the tactic response is the outcome of a temporal rather than a spatial sensing mechanism.[140] Thus, an *E.Coli* compares, with appropriately signed weight factors, the current attractant concentration with those a few seconds previously, and then 'decides whether to tumble or not';[26,109] note that the decision-making is only useful if it occurs in a time less than that taken for the direction of the run to de-correlate due to rotary diffusion, and this is the case since $\tau_0 D_r < 1$ (see §5).

5. Continuum Models for Collective Swimming

The discussion on continuum theories may be broadly divided into two classes. The first category in which work, both experimental and theoretical, started much earlier, concerns the phenomenon of bioconvection. The term was originally coined by[96] to refer to observations of pattern formation in suspensions of motile microorganisms[129] that bore resemblance to traditional Benard convection arising from an adverse temperature gradient. The second class of theories attempt to examine more recent observations of collective motion, at higher concentrations[38,133] and on smaller scales, mainly in suspensions of swimming bacteria.[115] The division is a natural one based on the underlying physics, since bioconvection patterns are the result of a density difference between the (heavier) swimmers and the suspending fluid coupling with the gravitational field; the means

The Biochemical Machinery for Chemotaxis

The modulation of the tumbling frequency in response to a changing attractant concentration essentially involves altering the bias between the clockwise (CW) and counterclockwise (CCW) states of motor rotation. This is achieved by a rather elaborate intracellular machinery, that exhibits a remarkably high gain—enough for the bacterium to perceptibly respond to a fractional change in the occupancy of membrane-bound receptors as small as 1/600).[13] Further, it allows the cell to respond to attractant concentrations ranging over several orders in magnitude. A schematic of the chemotaxis circuit is shown in fig. 11 and consists of two principal pathways.[89] The first involves four proteins (CheA, CheW, CheY and CheZ) and communicates between the receptors (known as methyl-accepting proteins -MCP's) and the flagellar motor. The second is responsible for cell adaptation and involves a pair of enzymes—a methyltransferase (CheR) and a methyl es-terase (CheB). The dimeric membrane-spanning receptors (shown as paired black wrench-like objects in the figure) form a ternary complex with two CheA and two CheW polypeptides and stimulate the autokinase activity of CheA (CheA $\rightarrow$ CheA-P; autophosphorylation). CheA-P transfers the phosphate to CheY, and CheY-P in turn interacts with the motor-switch complex to enhance CW flagellar rotation. Finally, the accumulation of CheY-P is prevented by CheZ, leading to an equilibrium in the absence of the attractant; that is, a baseline-bias between the CW and CCW states. Attractant binding inhibits the formation of CheA-P; the resulting dip in CheY-P levels suppresses CW rotation, leading to an increase in τ. In the adaptation pathway, CheR is responsible for receptor-methylation, while CheB-P, activated by phosphotransfer from CheA-P, removes methyl groups from the receptors. Thus, reduced CheA activity decreases the CheB-P level and the resulting increased methylation counteracts the attractant-induced inhibition. The time scales for ligand-binding and kinase (CheA) response are, however, much smaller than that characterizing receptor methylation (a few seconds). The inability of the methylation kinetics to (precisely) keep up with a continuously changing chemical environment manifests as a change in the fraction of bound receptors, leading to changed probabilities for the CW and CCW states. This lag manifests as the memory function characterizing the chemotactic response; one that may be determined from an impulse-response experiment. This has been done experimentally by Segall *et al.* (1986), and the resulting response function shown in fig. 12 underlies the temporal comparison (made by the bacterium) described above.

Figure 11: A schematic of the intracellular chemotactic signalling pathway. Reproduced from 'Bacterial locomotion and signal transduction', Manson, M.D., Armitage, J.P., Hoch, J.A. and Macnab, R.M., J Bacteriol, 1998, 180, 1009-1022.

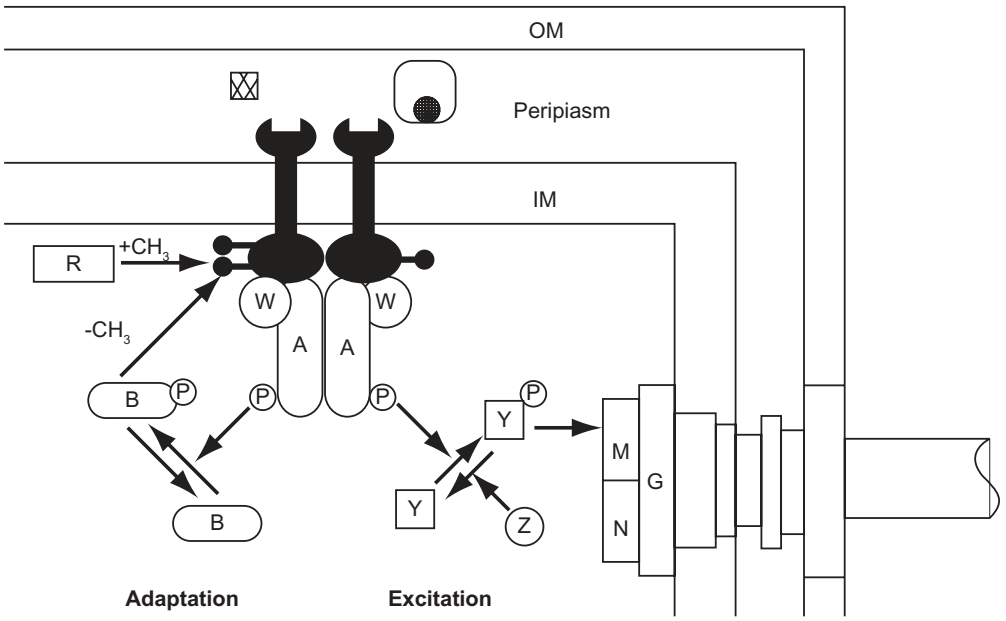

Figure 12: Impulse response to attractant in wild-type cells. The nature of the above response function may be understood as follows: The attractant concentration, in the vicinity of the bacterium, increases to begin with, raising the CCW bias of the flagellar motors, and stimulating receptor methylation. After the short but finite duration of the (experimental) pulse, the attractant concentration drops rapidly, and the still elevated methylation level causes the CCW bias to drop below pre-stimulus levels. In turn, this stimulates demethylation and the signal finally returns to its pre-stimulus level. Reproduced from 'Temporal comparisons in bacterial chemotaxis', Segall, J.E., Block, S.M. and Berg, H.C., Proc. Natl. Acad. Sci., 1986, 83, 8987-8991.

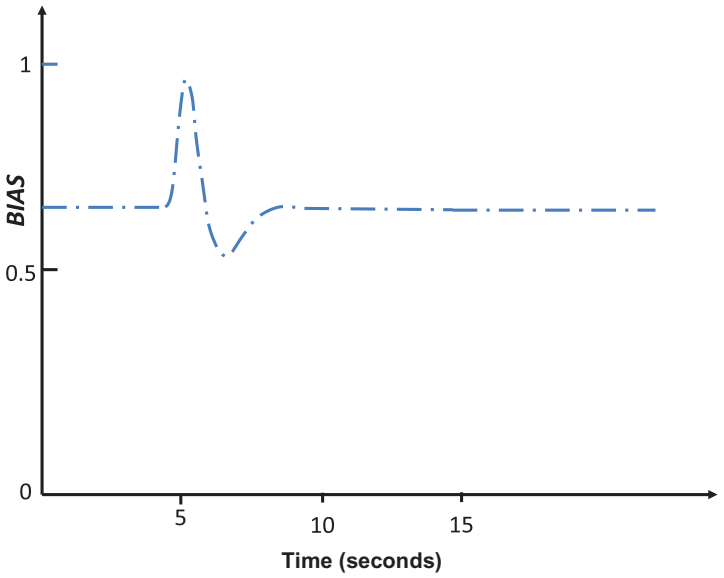

by which such a density difference leads to large-scale fluid motion could be any of geotaxis, gyrotaxis, phototaxis or chemotaxis. On the other hand, collective motion in bacterial suspensions is thought to arise due to the de-stabilizing effects of the intrinsic force-dipoles associated with individual swimmers at sufficiently high concentrations.

Figure 13 shows steady-state bioconvection patterns in a shallow suspension of motile algae viewed from both above and from the side.[95] One of the earliest theories[33] analyzed bioconvection as an overturning instability due to the adverse density gradient induced by heavier upward-swimming cells; see fig. 14. The upward swimming, an example of negative geotaxis, arises due to an asymmetric mass distribution—the algal cells (*C.nivalis*, *Euglena gracilis*, *Tetrahymena pyriformis* etc) are bottom-heavy and the resulting gravitational torque leads to an upward alignment of the swimming axis in the absence of a bulk flow. An exponential (algal) concentration profile is set up wherein convection due to upward swimming balances the downward diffusion; this base-state is (linearly) de-stabilized when the Rayleigh number, defined as $Ra = l^3(\phi\Delta\rho)g/(\mu D)$, exceeds a threshold value. Here, ϕ is the algal volume fraction, $\Delta\rho$ is the density difference between the alga and the suspending fluid, g is the gravitational acceleration, μ is the suspending fluid

Figure 13: The top figure shows a steady-state labyrinthine pattern developed in a suspension of *D.teriolecta*, 6.8 *mm* deep, viewed from above; the cell concentration is about 2 x 10^6*cells/cm*^{3}. The bottom figure shows steady-state bioconvection, with bottom-standing plumes, in a deep (15 *mm*) suspension of *C.nivalis*, with a concentration of 10^6*cells/cm*^{3} viewed from the side. Reproduced from 'Hydrodynamic phenomena in suspensions of swimming microorganisms', Pedley, T.J. and Kessler, J.O., Annual reviews of fluid mechanics, 1992, 24, 313-358.

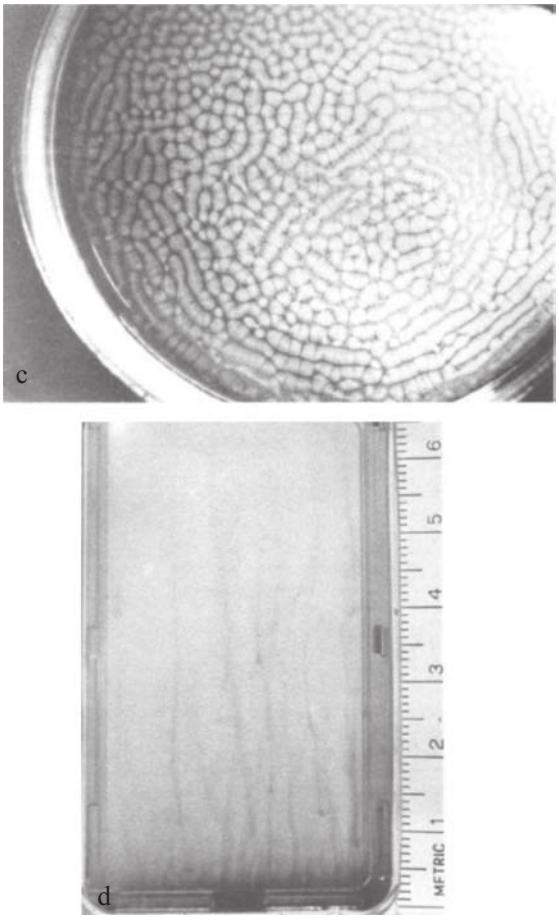

viscosity, and D is a measure of the cell diffusivity (of an athermal origin); the length scale l would either be the height H of the vessel in the limit of shallow layers, or the intrinsic length scale, D/U, characterizing the base-state stratification for sufficiently deep layers. An earlier effort by Plesset and Winet (1974) did recognize the driving force as being the unstable stratification induced by upward swimming; the analysis, however,[39] was along the lines of a Rayleigh-Taylor instability of an unstably stratified base-state with the dynamics of the swimming microorganisms not being explicitly accounted for. A second mechanism, relying on gyrotaxis rather than geotaxis, and acting to de-stabilize a homogeneous suspension, was proposed by Pedley, Kessler and co-workers.[54,93,94]

Taylor dispersion, named so after the British fluid mechanic G. I. Taylor, refers to the enhancement of the effective diffusion of a solute in a fluid due to coupling with a shear flow.

The Rayleigh-Taylor instability arises when the unstable equilibrium, involving a layer of heavier fluid above a lighter one, is perturbed. The instability results in the formation of plumes of the heavier fluid moving downwards through the lighter fluid.

Gyrotaxis refers to the directed swimming of a micro-organism under a balance of gravitational and viscous torques. As shown in fig. 14, an imposed density perturbation (a Fourier mode) induces a corresponding velocity perturbation since the fluid in the denser regions descends while rising in the ligher regions. The equilibrium orientation distribution arising from the resulting balance of viscous and gravitational torques drives a transverse gyrotactic flux of the heavier microorganisms into the denser regions, reinforcing the original density perturbation and leading to exponential growth.[141] A uniform unbounded suspension of gyrotactic swimming algae is always unstable to sufficiently long wavelength perturbations; the longest perturbations grow the fastest in the inertialess limit although, with inertia included, the growth rate attains a maximum at a finite wavenumber. For a bounded domain with a dimension H, an instability arises only when the critical wavenumber is greater than $O(H^{-1})$. This may be written in dimensionless terms as the threshold value of a gyrotactic Rayleigh number defined as $Ra_g = \mathrm{H}^2(UB)(\phi\Delta\rho)g/(\mu D)$, where $B = \mu/(2\rho\delta l\, g)$ is the time scale for alignment by the gyrotactic torque (δl here is the separation between the center of mass and the center of resistance, and varies from 1–5% of the characteristic cell dimension).[68] As to which of the two instabilities will occur in practice depends on the time scale on which the unstably stratified base-state (with a super-critical Ra) develops vis-a-vis the time scale on which a homogeneous suspension de-stabilizes due to gyrotactic fluxes. In either case, the actual sedimentation velocity of the algal cell due to the density difference is about two orders of magnitude smaller than the swimming speed, and may be neglected; this implies that the relative motion between an algal cell and the fluid occurs solely due to swimming.

The above analyses have since been extended in several different directions. For instance, the original analysis specified the upward swimming rate and the translational diffusivity in an ad-hoc manner. Later efforts attempt to rigorously relate these transport coefficients to the underlying orientation dynamics using generalized Taylor dispersion theory;[53,88] the flow-induced anisotropy in the translational diffusivity is found to affect linear stability predictions. The set of continuum field equations that support the aforementioned instability mechanisms, in their simplest form, may be written as:

$$\nabla \cdot \mathrm{u} = 0, \tag{6}$$

$$\rho\frac{Du}{Dt} = -\nabla p + nV(\Delta\rho)g + \nabla^2\mathrm{u}, \tag{7}$$

Figure 14: A schematic illustration of the two principal instability mechanisms leading to bioconvection patterns. The top figure illustrates the overturning instability arising due to negative geotaxis, while the bottom figure depicts the mechanism involving gyrotactic fluxes, in a direction transverse to gravity, that destabilizes a uniform suspension.

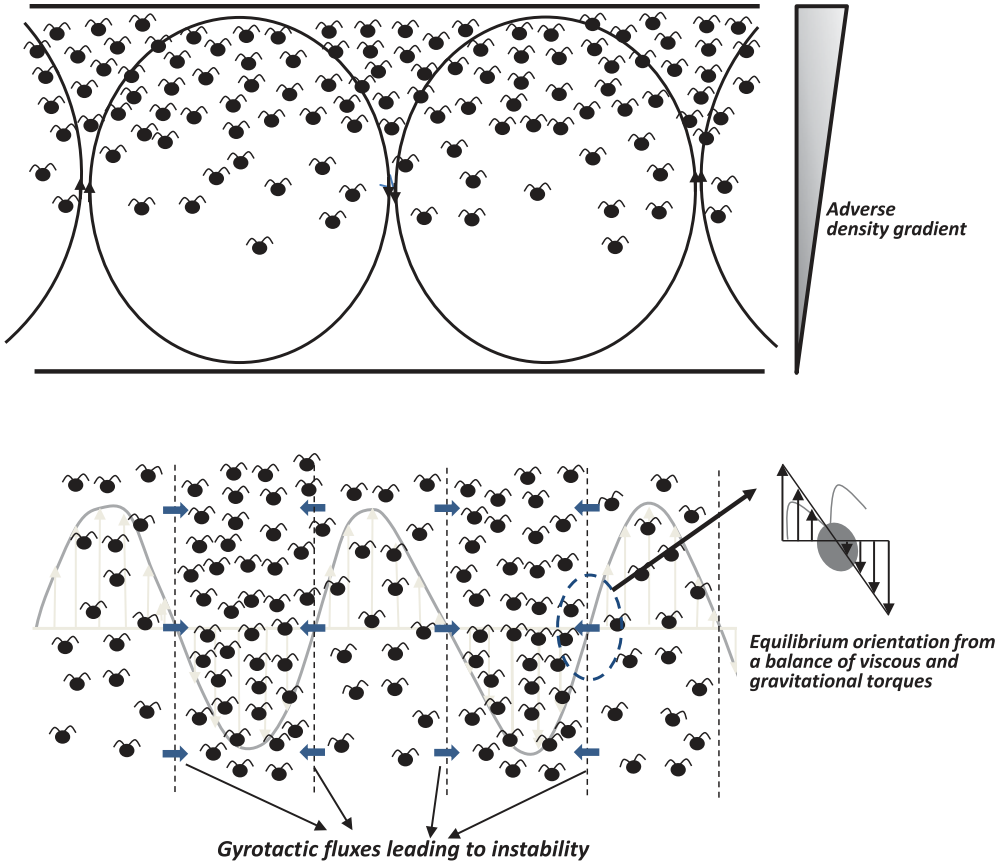

$$\frac{\partial n}{\partial t}+\nabla\cdot\left[n(\mathrm{u}+U\langle \mathrm{p}\rangle)\right]=\nabla\cdot(\mathrm{D}\cdot\nabla n), \qquad (8)$$

where $n(\mathbf{x}, t)$, $\mathbf{u}(\mathbf{x}, t)$, and $p(\mathbf{x}, t)$ are the averaged number density, velocity, and pressure fields, respectively, $\mathbf{g}$ is the gravitational force per unit mass, and V is the volume of an 3 individual swimmer. The orientation-averaged swimming velocity, $U\langle \mathrm{p}\rangle = U\int \mathrm{p}\Omega(\mathrm{p}, t)\,\mathrm{dp}$, that appears in the conservation equation for the number density, (8), may be determined from a knowledge of the orientation distribution function ($\Omega(\mathrm{p}, t)$) which, for gyrotactic algae, satisfies:

$$\frac{\partial \Omega}{\partial t}+\nabla_{\mathrm{p}}\cdot(\dot{\mathrm{p}}\Omega)=D_r\nabla_{\mathrm{p}}^2\Omega. \qquad (9)$$

Here, D_r is a rotary diffusivity that incorporates the intrinsically imperfect locomotion of the cells;[9] the convection in orientation space is given by the sum of the gyrotactic and viscous contributions:

$$\dot{\mathrm{p}}=\frac{1}{2B}[\mathrm{k}-(\mathrm{k}\cdot\mathrm{p})\mathrm{p}]+\boldsymbol{\Omega}\cdot\mathrm{p}+\mathcal{F}(\kappa)[E\cdot P-P(\mathrm{E}:\mathrm{pp})] \qquad (10)$$

The calculation of $\mathbf{D}$ in (8) is more complicated and involves determining the long-time spatial dispersion arising from the (orientationally averaged) dynamics in a primitive $(\mathbf{x}, \mathbf{p})$ phase space.

Experiments on bioconvection[8,69] show that the steady bioconvection patterns that are set up eventually have a considerably smaller wavelength than those characterizing the incipient instability. In general, the dominant length scale decreases with time with a concomitant change in the pattern topology; the length scale of the incipient pattern is closer to the predictions of the linear theory. These obserations have motivated non-linear extensions of the original analyses.[10]

Simulations have attempted to capture the structure, evolution and instability of gyrotactic plumes, in the fully developed regime, both in two and three dimensions.[45–47] Finally, it is worth noting that, in many cases, bioconvection patterns are the result of heavier cells undergoing photo or chemotaxis rather than geo or gravitaxis. In other words, the unstable stratification is set up due to gradients of a chemical (oxygen) or light intensity. The mechanistic details are different in these cases, and often more complicated.[55,56] In the case of *B. subtilis*, where the adverse density gradient is the result of oxytaxis (the slightly denser bacteria swim up an oxygen-gradient towards the free surface), an analysis would have to account for the coupling between the bacterial number density and oxygen concentration fields, since the oxytactic drift is, at leading order, proportional to the oxygen concentration gradient.[67] A second complication arises due to the bacterial cells being rendered inactive below a crtical oxygen concentration, leading to qualitative differences between the dynamics of shallow and deep layers. There have been similar attempts to analyze bioconvection resulting from phototaxis,[127] and a combination of both gyro- and phototaxis.[131]

The origin of the more recent work in the dynamics of suspensions of 'active' swimmers, in the absence of an external field (gravity), may be traced to the numerical simulations of Vicsek *et al.*,[126] described in §6; experiments with bacterial suspensions, demonstrating the existence of coherent motion in such active systems came later.[38,133] The simulations were a dynamical generalization of the classical *XY* model (with applications to superfluids and hexatic liquid crystals),[28] wherein each swimmer updates its orientation depending, in an averaged sense, on those of its nearest neighbors; much like the individual spins in the original equilibrium model. However, unlike the spins, the swimmers in Viscek's simulations also translate and thereby, sample a constantly changing environment. The most intriguing result to emerge from these simulations was the existence of a (continuous) order-disorder transition when the noise amplitude decreased below a critical level. The result is non-trivial because the simulations were restricted to two dimensions, in which case the Mermin-Wagner-Hohenberg theorem[28] prohibits the emergence of long-ranged order in the corresponding equilibrium model with a continuous order parameter.[142] Thus, the transition observed was believed to be characteristic of a system out of equilibrium. A later continuum theory by Toner and Tu[121,122] succeeded in predicting its occurrence. However, this effort and many others thereafter[15,50] are motivated by the need to characterize systems of active swimmers (which may range from microbes to birds!) in terms of appropriate non-equilibrium phase diagrams; the various phases arise, in a manner reminiscent of equilibrium systems, from short-ranged interactions between swimmers often specified in an ad hoc manner. Such analyses often have little to do with the fluid mechanics of a suspension of microorganisms interacting via long-ranged disturbance velocity fields.

Simha and Ramaswamy (2002) were the first to recognize the importance of long-ranged hydrodynamic interactions in a suspension of Stokesian swimmers, and via an appropriate set of continuum field equations, showed that such interactions would act to destabilize ordered 'active' phases. Thus, there can be no active analogs of the liquid crystalline nematic phase since, as shown in fig. 15, the perturbation flow driven by deviatoric active stresses act to enhance the amplitude of small-amplitude orientation fluctuations, leading to an exponential instability.[103] More recently, Saintillan and Shelley (2008ab) have shown that an isotropic swimmer suspension is again linearly unstable; crucially, an instability is predicted only for pushers, a fact that has been confirmed in simulations.[108,125] The instabilities of both ordered and isotropic phases owe their existence to the intrinsic force-dipoles associated with the swimmers.

While the above efforts highlight the intrinsic instability of active matter in general, relaxation mechanisms specific to most Stokesian swimmers, that could lead to a possible stabilization, were not included. The derivation of a threshold condition, similar to that obtained for bioconvection above, was first accomplished by Subramanian and Koch (2009) who obtained the critical concentration for the onset of collective motion in an isotropic bacterial suspension in terms of parameters (U, τ, $D_r, K(\mathrm{p}|\mathrm{p}')$; see the description of run-and-tumble dynamics in §3) that characterize the swimming motion of a single bacterium.

The set of continuum field equations for a bacterial suspension may be written as:

$$\nabla \cdot \mathrm{u} = 0, \tag{11}$$

$$-\nabla \mathrm{p} + \mu \nabla^2 \mathrm{u} - \frac{1}{2}\nabla \cdot \int \mathrm{dp}\Omega(\mathrm{x}, \mathrm{p}, \mathrm{t}) \times \int \mathrm{ds}\,[\mathrm{f}(\mathrm{p})\mathrm{sp} + \mathrm{spf}(\mathrm{p})] = 0, \tag{12}$$

$$\frac{\partial \Omega}{\partial t} + (U\mathrm{p} + \mathrm{u})\cdot\nabla_x \Omega + \nabla \mathrm{p}(\dot{\mathrm{p}}\Omega) = D_r \nabla_{\mathrm{p}}^2 \Omega - \frac{1}{\tau}(\Omega - \int K(\mathrm{p}\,|\,\mathrm{p}')\Omega \mathrm{dp}'), \tag{13}$$

Figure 15: The instability of an active nematic phase to a bend perturbation; the black arrows indicate the reinforcing flow induced by the orientation field perturbation.

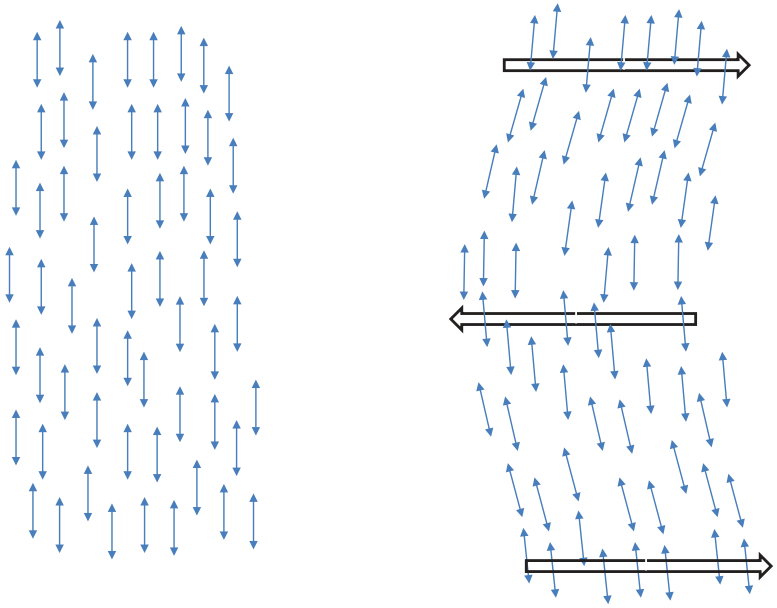

where the additional stress in (12) equals the density of force-dipoles.[143] This stress includes both an active contribution proportional to the orientational anisotropy of the intrinsic dipoles (this dipole has a magnitude of $O(\mu UL^2)$ with a numerical pre-factor, $\hat{C}$ (say), dependent on the detailed swimming mechanism) responsible for the instability, and the familiar passive contribution arising from the resistance of the swimmers to the local extensional action of the flow (the one that leads, for instance, to the enhanced viscosity of a suspension of passive fibers).[25] Equation (13) is the conservation equation for the phase-space probability density where the convection of probability in physical space due to swimming, and in orientation space due to rotation by an imposed flow field (the rotation rate being given by (5)), balances the relaxation processes of tumbling and rotary diffusion. The latter is modelled by an orientational Laplacian and denotes the gradual de-correlation due to small-amplitude orientation fluctuations during a run; in contrast, the large-amplitude tumble events appear as a non-local integral term. The effect of an instantaneous tumble is equivalent to a linear collision process—as in the kinetic theory of gases,[29] there is a change in the probability due to both 'direct' and 'inverse' events. The former denote a decrease in probability due to a tumble that causes a bacterium to leave the phase space interval of interest; for a Poisson process, this rate of departure equals $1/\tau$. The inverse events represent the increment in probability due to all tumbling events that lead to the final orientation of the bacterium lying in the interval of interest. In (13), the inverse events have been modelled using the transition probability density $K(\mathbf{p}\,|\mathbf{p}')$ that was introduced in §4 4.1, to allow a non-trivial correlation between the pre-tumble ($|\mathbf{p}'$) and post-tumble ($\mathbf{p}$) orientations.

A stability analysis using (11)–(13) in the dilute limit with an active stress contribution of $O(nL^3)$ (n being the bacterial number density), and about a quiescent isotropic base-state $\mathbf{u}_B = 0, \boldsymbol{\Omega}_B = \frac{n}{4\pi}$, leads to the following expression for the threshold bacterial concentration:[115]

$$(nL^3)_{crit} = \frac{\frac{30}{C\mathcal{F}(r)}\left(\frac{D_r L}{U}\right)\left[1+\frac{1}{2\tau D_r}\frac{(\beta\cosh\beta-\sinh\beta)}{\beta^2\sinh\beta}\right]}{\left\{1-\frac{15\mathcal{G}(r)}{C\mathcal{F}(r)}\left(\frac{D_r L}{U}\right)\left[1+\frac{1}{2\tau D_r}\frac{(\beta\cosh\beta-\sinh\beta)}{\beta^2\sinh\beta}\right]\right\}}. \quad (14)$$

where $\mathcal{F}(r)=\frac{(r^2-1)}{r^2+1}$ characterizes the orientation dynamics of an axisymmetric swimmer of aspect ratio r in a homogeneous shearing flow, and the function $G(r)$ is a measure of the bacterium inextensibility; with $K(\mathrm{p}\,|\,\mathrm{p}')=\frac{\beta}{4\pi\sinh\beta}e^{\beta(p\cdot p')}$ with $\beta>0$ accounting for the weak forward correlation observed in *E.Coli*.[11] Thus, for $nL^3 > (nL^3)_{crit}$, the quiescent state is susceptible to exponentially growing perturbations. Since tumbling typically dominates the orientation de-correlation of a swimming bacterium ($\tau D_r < 1$), and the correlation between pre- and post-tumble orientations is quite weak, a suspension of random tumblers ($\beta = 0, K(\mathrm{p}\,|\,\mathrm{p}')=\frac{1}{4\pi}; D_r = 0$) constitutes an important limiting case. The critical concentration in this limit is given by

$$(nL^3)_{crit} = \frac{\frac{5}{C\mathcal{F}(r)}\left(\frac{L}{U\tau}\right)}{1-\frac{5\mathcal{G}(r)}{2C\mathcal{F}(r)}\left(\frac{L}{U\tau}\right)}. \quad (15)$$

A suspension of slender-bodied straight swimmers ($D_r = 0$, $\tau \to \infty$) is thus always unstable ($(nL^3)_{crit} \to 0$). The above thresholds are entirely determined by the longest wavelength perturbations which are the most unstable.

The complete unstable spectrum for a suspension of straight swimmers is shown in fig. 16. The corresponding spectrum for random tumblers is obtained by merely displacing the straight-swimmer spectrum by an amount $1/\tau$ along the growth-rate axis; the spectrum with the inclusion of rotary diffusion instead of tumbling

has been obtained by Hohenberg and Shelley (2010). For straight swimmers, owing to the absence of any intrinsic time and length scales (other than the obvious microscopic ones: L/U and L), dimensional considerations lead one to conclude that the range of unstable wavenumbers must be $O(nL^2)$ with the corresponding growth rates being $O(nUL^2)$.

Figure 16 shows that there exist a pair of unstable stationary modes (modes 1 and 2 in fig. 16) in the wavenumber interval $\kappa < \kappa_m = 0.17\hat{C}nL^2$. The growth rate along one of these branches (Mode 2) is vanishingly small in the interval $\kappa \to 0$; the branch owing its existence crucially to the non-local nature of the swimming stress. In contrast, the growth rate of mode 1 remains finite in the limit of a vanishingly small wavenumber. This mode determines the threshold for instability in the presence of relaxation processes, and the underlying physical mechanism is depicted in fig. 17—an imposed (long-wavelength) velocity perturbation (Fourier mode) causes an excess (deficit) of swimmer orientations in the vicinity of the local extensional (compressional) axis. The disturbance flow associated with pushers in these orientations reinforces the original perturbation, leading to instability. Since the translation of the swimmers may be neglected in relation to the perturbation wavelength for $\kappa \to 0$, the resulting active stress is local and linear in the imposed velocity gradient. Thus, the dominant long-wavelength instability in a suspension of pushers may be interpreted in terms of a negative viscosity. For straight swimmers, the bacterial stress always exceeds the stabilizing viscous stress, associated with the suspending fluid, for sufficiently long wavelengths; leading to unconditional instability. In the presence of orientation de-correlation mechanisms, the amplitude of the bacterial stress is limited by the correlation time, either τ or D_r^{-1}, and instability requires a critical bacterial concentration. Although numerous experiments have demonstrated coherent fluid motion in bacterial suspensions, fewer have attempted to, either directly or indirectly, isolate a threshold concentration. One such experiment is by Wu and

Figure 16: The unstable spectrum for a suspension of straight swimmers. The shaded region in the $\hat{\alpha}_i$-k$ plane denotes the neutrally stable continuous spectrum modes. The mode 1 branch denotes the dominant instability in the limit of small wavelengths. Reprinted with permission from Subramanian, G., Koch, D.L. and Fitzgibbon, S.R., Physics of fluids, 23, 041901, 2011. Copyright 2011, American Institute of Physics.

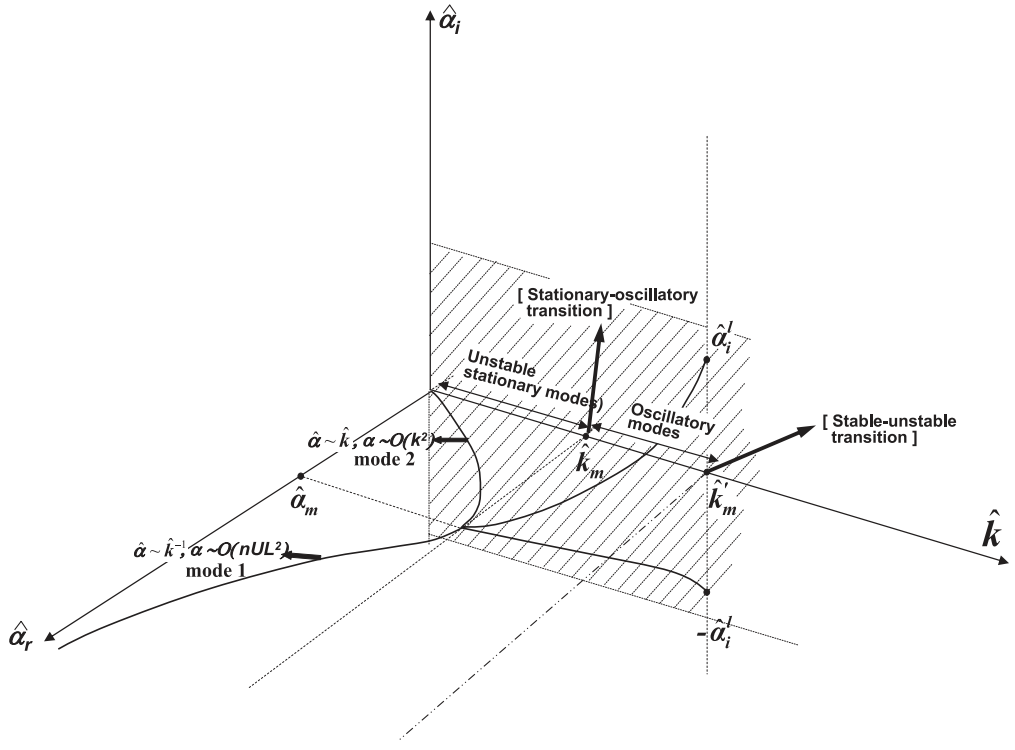

Figure 17: The long-wavelength instability of an isotropic bacterial suspension due to the coupling of velocity and orientation field fluctuations. Reproduced from Subramanian, G. and Koch, D.L., 2009, with permission from Cambridge University Press.

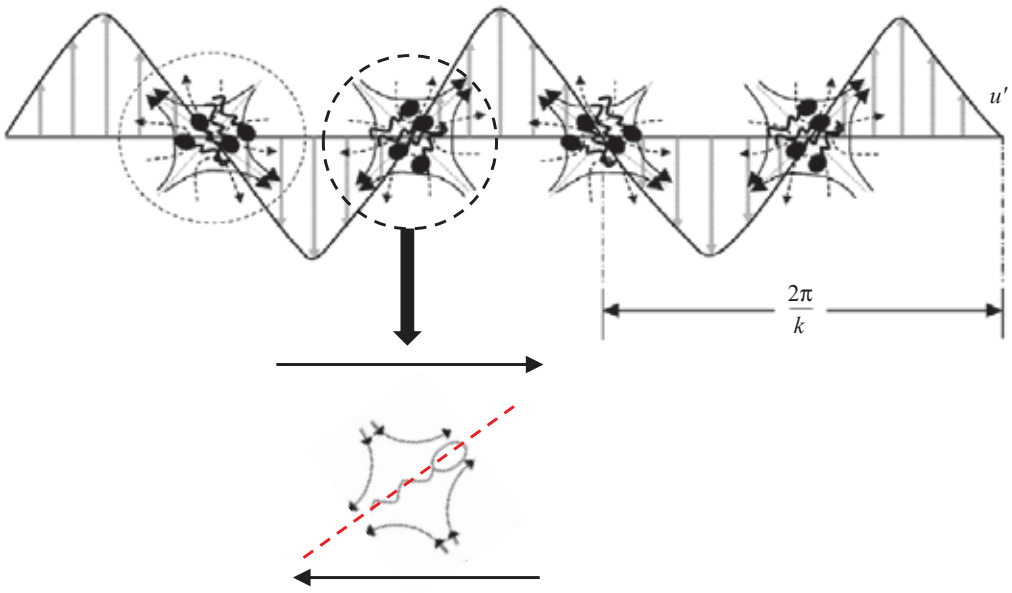

co-workers[132] who measured a large increase in the translational diffusion coefficient above a critical bacterial concentration in both suspensions of wild-type bacteria and smooth swimmers (that rotary diffuse but do not tumble); presumably due to additional convection of a swimming bacterium by the bulk fluid motion. Even in the stable regime, the bacterial suspension viscosity must decrease with increasing concentration (the threshold corresponding to a zero net viscosity) in sharp contrast to passive-particle suspensions; a fact originally pointed out by Hatwalne *et al.*(2004), and recently verified in experiments.[113]

Stationary unstable modes only exist for $\kappa < \kappa_m = 0.17\hat{C}nL^2$; at $\kappa = \kappa_m$, with $\kappa_m = 0.027\hat{C}nL^2$, they bifurcate into a pair of oscillatory modes in the range $\kappa_m < \kappa < \kappa'_m$ with $\kappa'_m = 0.57\hat{C}nL^2$. The existence of oscillatory modes (overstability) is important since, in practice, the domain is never infinitely large. In simulations, for instance, a lower boundon the wavenumber is provided by the box size, and for box sizes smaller than $2\pi/\kappa'_m$, one expects the onset of instability via an oscillatory mode. The physical interpretation of the instability is the simplest in the long-wavelength limit when the stationary orientation wave is out-of-phase with respect to the velocity wave; further, as shown in fig. 17, a single such wave suffices since the 'shape' of the orientation perturbation at all points in space is an ellipsoid with its major axis aligned along the local extensional axis. For any finite wavelength, however, one has a continuum of such orientation waves, each centered around a particular orientation, and with a unique phase difference with respect to the velocity wave that depends on the distance covered by a swimmer with the chosen orientation (in a time of the order of the inverse growth rate) in relation to the wavelength. As a result, there exist regions of space with subsets of force-dipoles acting in opposition to the local extension. When these regions become sufficiently large in extent, one expects oscillatory behavior since the force-dipoles would be in opposition to the local extension over a certain phase of the cycle; the analysis shows the critical wavenumber for oscillatory dynamics to be $0.57\hat{C}nL^2$. The spectrum terminates at $\kappa = \kappa'_m$ when growth rate is identically zero, and the discrete modes merge with the continuous spectrum (see below). The complete absence of modes beyond $\kappa = \kappa'_m$ has to do with neglect of fluid inertia, and therefore, of momentum relaxation processes not directly driven by stress perturbations; these would otherwise decay on a time scale of $O(\nu\kappa^2)^{-1}$.

Although the analysis above predicts a dilute suspension of straight swimmers to be unstable, it turns out, rather interestingly, that the inclusion of pair-hydrodynamic interactions allows, in principle, for a stabilization to long wavelength perturbations. Such a non-trivial stabilization, at

$O(nL^3)$,[144] is particularly relevant to simulations of swimmer suspensions almost all of which have focussed on straight swimmers (see §6). The possibility arises because time scale of the instability is $O(nUL^2)^{-1}$, being inversely proportional to the (intrinsic) dipole density, while the relaxation, on account of a pair-interaction induced rotary diffusivity of $O(nUL^2)$, also proceeds on the same time scale[145] It was shown by Subramanian and Koch (2009) that the stabilizing effect of pair-interactions is too small for high-aspect-ratio swimmers. However, the amplitude of the de-stabilizing active stress weakens (slender-bodied swimmers are the most sensitive to the orienting effects of an ambient extensional flow) and the rotary diffusivity increases with a decrease in aspect ratio (pair-interactions are logarithmically weak in the slender body limit). There must eventually be a balance for a critical aspect ratio, greater than unity, when a dilute suspension of pushers becomes stable. According to this argument, a suspension of spherical swimmers, those examined by Pedley and co-workers, is certainly stable. A spherical squirmer responds solely to the ambient vorticity, and an isotropic distribution of squirmer orientations remains undistorted in the presence of an imposed velocity perturbation. Thus, it appears as if the pattern formation observed in the simulations of Pedley and co-workers requires an alternate explanation; one that likely relies on the nature of the detailed interactions in the near-field rather than the universal picture, based on far-field dipole interactions, described above.

A remarkable feature of the mechanism depicted in fig. 17 is that it allows for an instability arising from the favourable coupling of velocity and orientation fields alone. The corresponding number density field remains spatially homogeneous! This is, of course, in sharp contrast to bioconvection patterns where the unstable bulk motion is driven by gradients in the algal number density; the concentration within falling gyrotactic plumes in the fully developed state is often an order of magnitude higher than its average value of $O(10^6$ cells/ml). Although, for exceptional initial conditions, a bacterial suspension would remain homogeneous for all times while still supporting an exponential instability, a natural question arises as to what happens of the number density (concentration) fluctuations, on length scales larger than microscopic (bacterium length), that are present in, or derive from, a general initial condition. This is also an important question in light of the results of Sain-tillan and Shelley (2008) obtained from simulations of the field equations in the non-linear regime. In stark contrast to the linear stability analysis, the simulations reveal large-scale concentration inhomogeneities. While the observed concentration fluctuations may have a non-linear origin, an understanding of the evolution of such fluctuations in the linearized setting is nevertheless essential. This may be achieved by considering the complete eigen-spectrum of a bacterial suspension rather than focussing on only the unstable spectrum in fig. 16. For a suspension of straight swimmers, the discrete spectrum consists solely of the unstable modes which are spatially homogeneous; the evolution of the number density field is thus governed by neutrally stable propagating singular modes that make up the continuous spectrum. Despite a finite relaxation time, a singular continuous spectrum persists for random tumblers now comprising stable modes that decay on a time scale of $O(\tau)$. The singularity arises because any orientational anisotropy, regardless of angular scale, decays on the same time scale (τ); using $K(\mathrm{p}\,|\,\mathrm{p}') = \frac{1}{4\pi}$ in (13), τ is seen to be an infinitely degenerate eigenvalue. The existence of a continuous spectrum, and the associated non-normality, implies that even linearized concentration fluctuations may exhibit transient growth although the individual eigenmodes are stable;[146] the transient growth, for sufficiently amplitudes, might eventually trigger non-linearity.

The analysis leading to the critical concentrations ((14) and (15) above) is valid only in the dilute limit, when each bacterium responds to an imposed perturbation flow independent of its neighbors; the imposed flow must itself be regarded as the consequence of the long-ranged dipole fields of distant bacteria. At the concentrations relevant to experiments ($n \sim 10^9$ *cells/ml*; with $L \approx 10\,\mu m$, the hydrodynamic volume fraction $nL^3 \approx O(1)$), however, one expects hydrodynamic interactions between neighboring bacteria to assume significance. As for passive suspensions, the dilute non-interacting scenario must arise, at leading order, in an expansion in nL^3 in which successive terms account for interactions between increasing numbers of particles.[58] The first correction is due to pair-interactions, a consequence of which was already examined in the context of straight swimmers above. One may quantify the effects of such interactions in terms of a pair distribution function that would depend on the microscopic swimming mechanisms and on the nature of the relaxation processes. For instance, the pair-interactions are expected to differ essentially in suspensions of pushers and pullers as evidenced in recent simulations.[108] A calculation of the pair distribution function would

mirror, in a conceptual sense, similar efforts for passive-particle suspensions where Brownian motion serves as the relaxation mechanism,[4,5,21] and will thereby allow a comparison of active and passive systems on the same footing. At the present time, however, computations of the pair-distribution function only exists for the case of spherical squirmers[61] and flagellates[90] based on the detailed pair-trajectories.

Although beyond the scope of the present review, it is worth noting that recent analyses have begun analyzing the dynamics of a bacterial suspension in a changing chemical environment. For instance, Subramanian *et al.*[116] have examined the onset of instability in the presence of an imposed chemo-attractant gradient that leads to an anisotropic base-state. Instability is now predicted to occur at a lower concentration with the dominant mode continuing to support a spatially homogeneous number density field. Motivated by the recent experiments of Goldstein (2009), wherein a qualitative change in the dynamics was observed, in a suspended film of *B.subtilis*, beyond a certain critical film thickness, Kasyap and Koch (2011) have examined the instability of a suspension of chemotactic bacteria driven by concentration fluctuations. In general, however, efforts that have attempted to combine chemotactic and hydrodynamic fluxes model the former response in a rather simplistic fashion.[57,116] On the other hand, efforts that rigorously examine the role of chemotaxis in large-scale pattern formation typically neglect hydrodynamics;[16,26] particularly, the flow driven by chemotactic stresses. It is clearly desirable to develop a consistent formulation that models both hydrodynamics and chemotaxis at the same level of detail. In this regard, we note that a system-level description of an *E.Coli*, acting as a bio-chemical signal processor, has been developed recently by Berg and co-workers.[123]

6. Discrete Simulations for Collective Swimming

We have seen in §5 that continuum models are useful in understanding the behaviour of swimmer suspensions at length scales large compared to their size. However, their success depends on the accuracy of the relations for the fluxes of the number density and swimmer orientation, and the suspension stress. For a suspension that is dilute enough that the swimmers do not interact, the problem simplifies considerably—the results discussed in §5 pertain to this limit. The problem becomes more complex when the swimmer concentration increases to a level that interactions may not be ignored. This is indeed the case in experiments with bacterial suspensions, since large-scale coherent motion is typically observed when the hydrodynamic volume fraction nL^3 is $O(1)$. For suspensions of passive particles, interactions become important at fairly low concentrations; for spherical particles, analytical expressions for the stress that account for interactions have been given, starting from Batchelor & Green,[6] but are restricted to pair interactions and are valid only for low concentrations. For concentrations of swimmers of practical relevance, the difficulty of capturing the many-body hydrodynamic interactions and the statistics of particle configurations make the formulation of exact analytical relations onerous, if not impossible. In these situations, discrete simulations have the potential of providing useful information and insight.

Perhaps the first discrete simulation of collective dynamics was the study Vicsek *et al.*;[126] the theoretical underpinnings of this and related continuum models that appeared later were discussed briefly in §5. The authors completely eschewed detailed hydrodynamics, and proposed instead a model in which the positions of the 'self-driven particles' (Vicsek *et al.* sought to address the collective motion of all motile 'particles', not just microorganisms swimming in a fluid) were updated according to a simple set of rules: each particle moves with constant speed, and its orientation at any time step is the average of the orientations of other particles in its neighbourhood in the previous time step, with a random noise added. This simple model leads to a range of behaviour, including a continuous transition from a disordered 'phase' to an oriented phase with increasing number density and/or decreasing noise. The study has led to many others that have used it as a model for "flocking" and coherence.

In the recent past, several studies have developed models for simulating the collective dynamics of swimming microorganisms, which take account of hydrodynamic interactions to varying degrees of accuracy. Figure 18 shows schematic illustrations of some of the models. The fundamental relations governing the motion of the swimmers in all the models are the same, namely that the net torque and force vanish on each swimmer. From the linearity of Stokes equations (1), these may be written as

$$\sum_j \boldsymbol{A}_{ij} \bullet \left(\boldsymbol{u}_j - \left\langle \boldsymbol{u}_j \right\rangle \right) + \tilde{\boldsymbol{B}}_{ij} \bullet \left(\boldsymbol{\omega}_j - \left\langle \boldsymbol{\omega}_j \right\rangle \right) = 0, \qquad (16)$$

$$\sum_j \boldsymbol{B}_{ij} \bullet \left(\boldsymbol{u}_j - \left\langle \boldsymbol{u}_j \right\rangle \right) + \boldsymbol{C}_{ij} \bullet \left(\boldsymbol{\omega}_j - \left\langle \boldsymbol{\omega}_j \right\rangle \right) = 0, \qquad (17)$$

where u_j, Ω_j are the linear and angular velocity of swimmer j, and $\langle u \rangle_j$, $\langle \Omega \rangle$ are the velocity and

vorticity of the fluid at the centre of the particle *j*. Here $\boldsymbol{A}_{ij}$, $\tilde{\boldsymbol{B}}_{ij}$, $\boldsymbol{B}_{ij}$ and $\boldsymbol{C}_{ij}$ are resistance tensors[72] that relate the force and torque on particle i to the velocity and angular velocity of particle *j*. The differences between the various models lie in the forms of the resistance tensors, due to the differences in the shape and construction of the swimmers, and the level at which interactions are computed. The method of Ramachandran *et al.*[102] (fig. 18d) does not determine the swimmer trajectories by calculating the resistances, but by determining the velocities at every node (see below).

Hernandez-Ortiz *et al.*[52] proposed a simple model for a collection of self-propelled swimmers, wherein each swimmer is a dumbbell comprising two spheres held together by a virtual rod that imposes the constraint of rigidity. Propulsion is effected by a 'phantom' flagellum attached to one of the spheres. The dumbbells interact through the fluid velocity disturbances they cause, which are determined by treating the component spheres of each dumbbell as point forces, an approximation that only holds in the limit $nL^3 \ll 1$. They showed evidence of the preferential migration of swimmers (pushers) toward the walls, in agreement with earlier observations for spermatozoa,[106] and more recent ones for *E.Coli*.[14] Using this model, Hernandez-Ortiz *et al.*[51] determined the self diffusivity of a collection of swimmers confined between two plane walls, the results of which are displayed in fig. 19.[147] Underhill *et al.*[125] carried out simulations for a periodic domain, and highlighted crucial differences between suspensions of puller and pushers; in particular, the tracer diffusivity in a suspension of pushers exhibits a strong system-size dependence.

A more consistent and accurate method for the computation of swimmer interactions was introduced by Saintillan & Shelley[108] who used slender body theory to determine the swimmer velocity disturbances and the motion of an individual swimmer in response to such disturbance fields. They prescribed a force distribution on either the fore- (puller) or aft- (pusher) portion of the swimmer, while allowing for an (unknown) tangential slip—this models the propulsion apparatus. A no-slip boundary condition was imposed on the remaining portion of the swimmer with the requirement that the

Figure 18: Schematic figures depicting the various swimmer models. The first two are for slender, or rod-like, swimmers, and the next three are for sphere-like swimmers. In all the models, the single arrow gives the director, or the direction of swimming of a free swimmer. (a) Hernandez-Ortiz *et al.*[52]: the arrows indicate the force imparted by the 'phantom flagellum' on the upper sphere (outward for pullers, and inward for pushers). (b) Saintillan & Shelley[108]: in the orange part of the rod, a tangential force $\boldsymbol{f}_0$ per unit length is applied (as caused, for example, by undulating cilia), and a tangential slip velocity is allowed. In the the blue part, the no-slip condition is enforced. (c) The squirmer model of Lighthill,[83] as applied by Ishikawa *et al.*[63]: The red arrows on the surface indicate the direction of the squirming velocity. (d) Ramachandran *et al.*[102]: The black circles are the lattice points outside the swimmer. The filled red and blue circles are the lattice points in the interior of the swimmer, from which momentum is externally injected and taken away, respectively. (e) Mehandia & Nott[90]: The dot inside the swimmer represents the point of action of the fixed stresslet $\boldsymbol{S}_0$, that is responsible for propulsion.

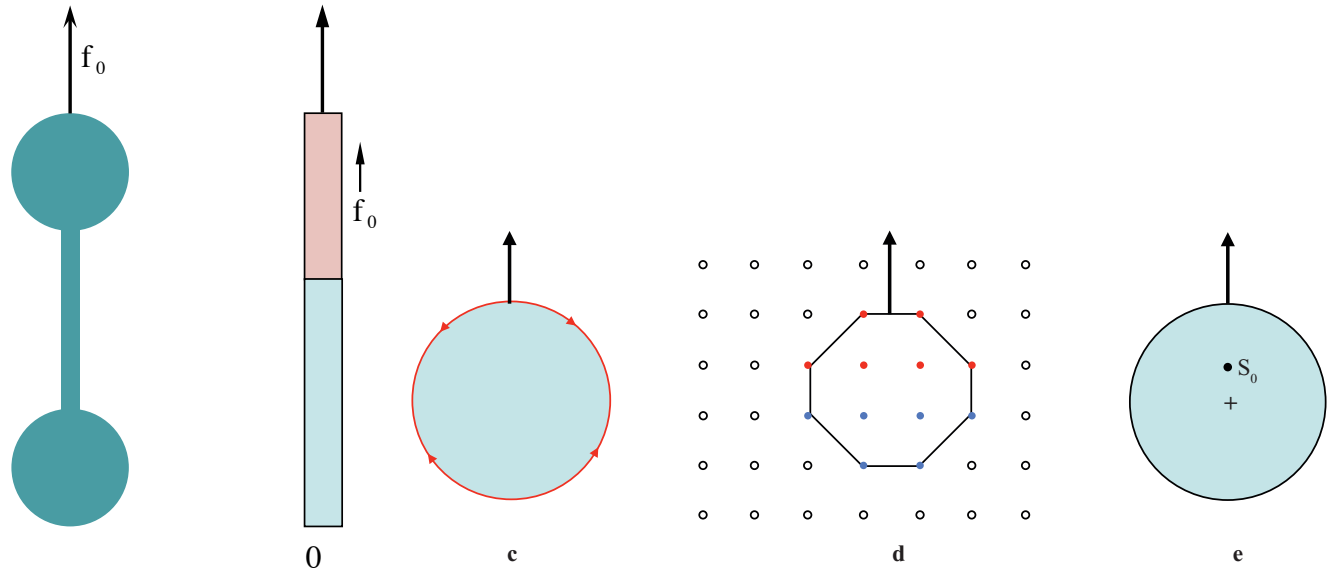

net force on the swimmer vanish, so a swimmer acts as a force-dipole on large length scales. The method exploits the framework of slender body theory to leading logarithmic order, and is thus accurate to $O(\log(a/L)^{-1})$, where a is the lateral dimension of the swimmer and L its length.[148] The formulation provides an accurate description provided the majority of swimmer interactions occur at separations much greater than a; an assumption that is likely to remain valid in the semi-dilute regime $nL^3 \gg 1$, $nL^2a \ll 1$. The simulations showed that an initial configuration of aligned swimmers rapidly becomes orientationally disordered, thereby confirming the predictions of Simha & Ramaswamy[112] on the instability of ordered active phases. For large times, an isotropic state results on suffciently large scales, although interactions between neighboring swimmers leads to a persistence of local orientational order. The authors also determined the rotary and translational diffusivities as a function of nL^3. Rather surprisingly, despite the onset of large-scale coherent motion, the two diffusivities were found to be related as $D_t = U^2/(6D_r)$, obtained from Taylor dispersion theory for orientable Brownian particles in an otherwise quiescent medium. This is perhaps an indication that orientational de-correlation due to the fluid velocity gradients dominate the dispersion behavior. Further, D_r was found to be directly proportional, and D_t inversely proportional to the swimmer concentration, a behavior also anticipated from pair-interactions in a quiescent medium; however, the numerical pre-factors were much larger than those obtained from a pair-interaction calculation.[115]

The studies discussed above aimed to simulate the collective behaviour of rod-like swimmers such as *E.Coli*. A few methods have also emerged to simulate swimmers of other shapes. Ishikawa *et al.*[63] used a particular version of the Lighthill-Blake model to simulate suspensions of spherical squirmers (see §III). Assuming a surface motion that is axisym-metric (about the axis defining the direction of swimming), the boundary condition for the tangential surface velocity takes the form[83]:

$$u_\theta = \sum_{n>0}^{\infty} \frac{2B_n}{n(n+1)} \sin\theta P'(\cos\theta) \qquad (18)$$

where P_i is the *ith* Legendre polynomial, and θ is the polar angle measured from the swimming axis. The surface velocity in the radial direction is assumed to be zero. The solution of the Stokes equations with the above boundary condition yields the velocity and pressure fields (which we do not reproduce here) induced by a squirmer. Simulations have been carried out in the dilute regime[60,61] assuming pair interactions, and in the concentrated regime[62] by a modification of the Stokesian dynamics protocol[22] (a brief description of which appears below)—they determine the effect of squirmer interactions on the large-scale dynamics. While the method is, in principle, sound, the model used in the simulations terminates the series in (18) at the second term. For a pusher, this has the undesirable feature of a reversal in the surface velocity near the rear stagnation point for $B_2/B_1 > 1$ (the reversal, for a puller, first occurs at the front stagnation point). The results obtained, with regard to the diffusion and rheology of a squirmer suspension, appear sensitive to the above artifact. Although the connection between the particular spherical squirmer examined and a real ciliate appears to be a tenuous one,[59] one may nevertheless use the squirmer model, with a varying surface velocity profile, to examine the effects of the varying nature of (near-field) hydrodynamic interactions on the bulk suspension characteristics. This would help complement continuum theories that have largely been based on far-field interactions.

Ramachandran *et al.*[102] developed a model swimmer using the lattice-Boltzmann method (LBM) which has already been applied quite successfully to Stokesian suspensions of rigid passive particles.[75] Moreover, LBM has been shown to be scalable for parallel computation, and is therefore an effective computational tool for modern computers. Ramachandran *et al.* effected self-propulsion by removing momentum from the fluid nodes on the aft side of the swimmer and adding the same amount to the nodes in the fore side of the swimmer (but in an asymmetric manner), thereby inducing a force-dipole. Llopis & Pagonabarraga[85] used this model to simulate interacting swimmers; however, they choose a particle spanning only a few lattice points, making the spatial discretization very coarse. As a result, the method was unable to capture the hydrodynamic interactions at close approach. Further, they assumed an elastic collision between particles, which differs qualitatively from the dissipative nature of short-ranged hydrodynamic interactions in the inertialess limit. Choosing a suffciently fine grid for computation of the interactions with acceptable accuracy increases the computational cost beyond current capabilities—this appears to be a drawback of LBM for suspensions. Nevertheless, LBM is potentially a useful method for the simulation of microorganism suspensions, as it can be adapted relatively easily to include inertia, non-Newtonian fluid rheology and other complexities.

The final method we discuss is that of Mehandia & Nott,[90] who approximated the swimmer as a sphere, and effected propulsion by placing a force dipole displaced from its geometric centre.[149] They modified the Stokesian Dynamics method, which is used widely for the simulation of Stokesian suspensions[20,92,111] to incorporate self-propulsion. In the original method, the fluid velocity disturbance due to each particle is computed as a truncated multipole expansion of the force densities on the particle surface about its centre. To incorporate the off-centre stresslet in this formalism, it has to be translated to the geometric centre of the particle—this will, in principle, introduce all higher-order multipole contributions. To make a simplification that will truncate the multipole expansion at the dipole, Mehandia & Nott calculated the propulsion velocity of each particle as though it was produced by an external force; however the velocity disturbance, that would govern swimmer interactions, was computed as that of a stresslet. This approximation is equivalent to the use of the phantom flagellum by Hernandez-Ortiz *et al.*[52] At high swimmer concentrations, this approximation causes an error in the self-mobility that needs further examination. On the other hand, the method computes the near-field interactions between swimmers more accurately than the other studies discussed above, thereby allowing suspension properties to be determined even at relatively high concentrations.

Figure 19 shows that the simulations based on the diverse swimming models share a common feature of the translational diffusivity D_t of the swimmers decreasing algebraically with the number density, and roughly as $D_t \propto n^{-1}$. The actual numerical values for the different methods differ widely, due to differences in the shapes of the swimmers used and some imposed constraints (Hernandez-Ortiz *et al.*[52] confined the swimmers between plane parallel walls, and Mehandia & Nott[90] confined their motion to a plane); moreover, the different simulation methods capture interactions to varying degrees of accuracy, as described above. Now, a decrease of D_t with n would, in the absence of bulk fluid motion, arise due to the absence of relaxation mechanisms. This is because pair-interactions act to cut-off the ballistic trajectories of straight swimmers, and the resulting 'swimmer mean free path' is $O(1/(nL^2))$ for small n; the corresponding translational diffusivity must therefore be $O(U/(nL^2))$. However, the decrease with n in fig. 19 is over a range of concentrations that apparently lie in an unstable regime characterized by large-scale coherent fluid motion. An inverse dependence on n, in this regime, is by no means obvious, and one expects the accompanying numerical pre-factor to differ from that corresponding to pair-interactions in a stable (quiescent) state. That this is the case for the simulations of Saintillan and Shelley (2007) has already been verified.[115] Simulations are, however, yet to reveal a transition from the stable to the unstable regime as a function of either the swimmer concentration or domain size. In contrast, experimental observations of swimming *E.coli*.[132] on account of intrinsic relaxation mechanisms, show that D_t increases sharply with n before decreasing at much higher concentrations. Perhaps a greater deficiency of all simulations is that they do not account for the orientational relaxation naturally present in most wild-type Prokaryotes, namely tumbling. The run-and-tumble dynamics commonly observed, and even quantified for *E.coli*, has been ignored in all the methods. A very recent study[104] has attempted to redress this deficiency by incorporating tumbling; the author's observation that the diffusivity falls by almost an order of magnitude with the inclusion of tumbling is consistent with the data of Wu *et al.*[132] who found the translational diffusivities of smooth-swimming bacteria (that rotary diffuse but do not tumble) to be higher than those of

Figure 19: The self diffusivity as a function of swimmer concentration, as determined by four of the simulation methods described in the text. The dashed line of slope –1 is given for comparison. The diffusivity is scaled with $UL/2$, where L is the largest dimension of the swimmer (the length for a rod, and the diameter for a sphere). All the simulations display a roughly power-law decay of the diffusivity, but the numerical values differ by two orders of magnitude.

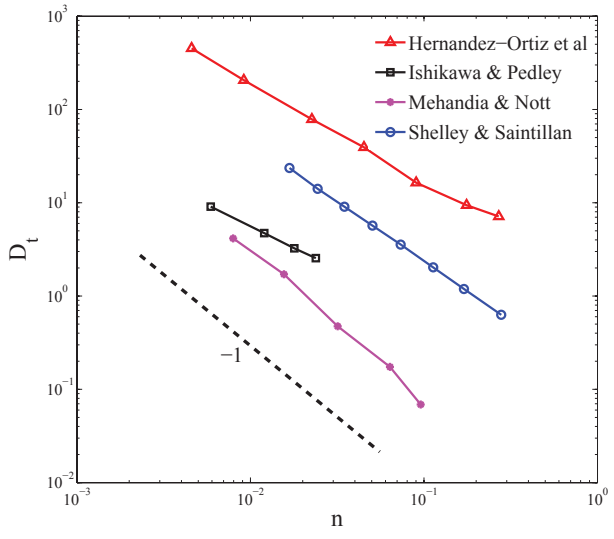

wild-type; the increase of the diffusivity with n is, however, not captured.

As elaborated in §4 A, chemotaxis in bacteria arises from a modulation of the tumbling frequency so as to lengthen the runs up the gradient of a chemoattractant. Reddy[104] incorporated such a modulation using the data of Brown & Berg[27] on the tumbling statistics *E.coli*, and conducted dynamic simulations over a range of swimmer concentrations. It was observed that the chemotactic drift decreases with increasing swimmer concentration—as the swimmer interactions in the simulations are purely hydrodynamic, this result implies that the orientation dispersion caused by hydrodynamic interactions attenuates the chemo-tactic response of individual cells. On the other hand, as shown by Subramanian *et al.*,[116] the large-scale flow driven by chemotactic stresses may reinforce the instability predicted in §5 for a homogeneous chemical environment; this might manifest as an increase in the swimmer velocity at higher (supercritical) concentrations. To our knowledge, experimental data on the chemotactic drift as a function of bacterial concentration has not been reported.

7. Summary and Conclusion

Given the vigorous research activity in this field and many ongoing developments, this review necessarily had to concentrate on a few themes. Our main intention is to give a flavour of the fluid dynamics of swimming microorganisms and living cells, and convey the important role that the fluid plays both in the motion of individual swimmers and in their collective motion as a group.

The first part of the review concentrated on the mechanics of individual swimmers. The discussion was limited to Stokesian swimmers, for which the Reynolds number based on the size and speed of the swimmer is vanishingly small; the non-trivial effects of fluid inertia were briefly mentioned at the end of §2. The constraints imposed by low *Re* were explained in §2, the primary one being that the swimming stroke be non-reciprocating; a hypothetical low-*Re* scallop was used as an illustrative example of reciprocating motion that does not result in swimming. Two simple but artificial swimming protocols, namely the Purcell and trumbbell swimmers, composed of straight links that either rotate about hinges or undergo sequential changes in length, were introduced as examples of non-reciprocating stroke kinematics. The moving appendages that provide thrust in real-life swimmers are neither straight nor rigid, but are flexible elastic filaments, flagella and cilia being the most widely prevalent. The details of the structure and kinematics of flagella and cilia, and the manner in which they generate thrust, were discussed in §3. The fluid motion caused by a swimmer, and its effect on the orientations of other neighboring swimmers were discussed, with a view of their application to discrete particle simulations of swimmer suspensions. Section 3 ended with a discussion on the run-and-tumble dynamics of prokaryotes, and how a modulation of the tumbling statistics, in a chemically heterogeneous environment, leads to the phenomenon of chemotaxis.

The latter part of the review focused on the large-scale dynamics in swimmer suspensions. Section 5 discussed continuum models in which conservation laws are written for the local averages of the orientation and number density of the swimmers, and the momentum density of the suspension. The averaged quantities that appear in the conservation equations may in turn be determined from an underlying kinetic equation for the probability density in position-orientation space. Two physically distinct applications of such models were elaborated upon. The first concerned the phenomenon of bioconvection that refers to the intricate patterns that form in shallow layers of suspensions of motile microorganisms. The continuum models show that these patterns arise from large-scale instabilities driven by a coupling between tactic responses (mainly a combination of gravitaxis and gyrotaxis) and the density difference between the swimmers and the suspending fluid. The theories offer a good qualitative explanation of the observed phenomena, but the predictions of the dominant length scales from a linearized analysis differ significantly from observations. The deviations may be due to non-linear effects, or more complicating physical factors in the experiments such as a gradient in the oxygen concentration. The second application of continuum models addressed more recent observations of velocity fluctuations and coherent motion on smaller scales, in experiments and dynamic simulations of (neutrally buoyant) bacterial suspensions. These instabilities were shown to result from a coupling between the orientation dynamics of individual rod-like swimmers in response to an imposed perturbation, and the resulting reinforcement of the perturbation. Crucially, the theoretical prediction of an instability applies only to a suspension of pushers, and for concentrations above a critical value determined by intrinsic relaxation mechanisms.

Section 6 discussed discrete models developed for the study of suspensions of swimmers. Each swimmer is tracked as a function of time, and bulk properties determined by appropriate averaging. The equations governing the motion

of a neutrally buoyant swimmer are that the net force force and torque are zero. The physical models and computational methods used for discrete simulations are diverse. The simplest completely disregards hydrodynamics and instead uses simple rules for the evolution of the swimmer trajectories,[126] motivated by pedagogical models originally used to understand phase transitions. A variety of methods have since been used that build in more realistic models for propulsion, while also accounting, to varying degrees of accuracy, for hydrodynamic interactions between swimmers in a fluid medium.[52,62,63,90,102,108] Some of these are limited to far-field hydrodynamic interactions between rod-like swimmers, and thereby to low concentrations.[52,125] Others have used slender body theory to include interactions between such swimmers on length scales of the order of the swimmer length, thereby extending the range of validity possibly to concentrations in the semi-dilute regime.[108] Other methods[62,90,102] account for detailed hydrodynamic interactions in suspensions of spherical swimmers, at distances comparable to the swimmer size, but they suffer from other limitations. The main applications and results of the discrete models were discussed. The simulations of suspensions of rod-like swimmers[52,108,125] qualitatively reproduce predictions of the continuum models, such as an instability of an initially aligned swimmer suspension, and the emergence of large-scale coherent motion for pushers from an initially isotropic state. Only one very recent study[104] has incorporated the effects of tumbling and its chemotactic modulation on swimmer dynamics, but the authors have not studied large enough systems to enable meaningful comparisons with predictions of continuum theories or experiments.

Perhaps the most important aspect of the microorganism behaviour that this review leaves out is their social behaviour resulting from chemical sensing, which is responsible for phenomena such as quorum sensing, the formation of biofilms, and cell differentiation in colonies. Even relatively small and simple bacteria like *E.coli* have an elaborate array of chemoreceptors on the membranes that bind to some sugars, amino acids and a few other small molecules. By this mechanism, they seem to sense their population density in the suspension—the sensing of sugars is relevant for chemotaxis (see boxed text in page 20), and the sensing of endogenously produced molecules called autoinducers, is responsible for social behaviour. Large strides have been made in understanding the biochemical pathways that control the sensing and production of the autoinducers, but much remains to be done in understanding the kinetics of the reactions and their relation to interactions. The coupling of the kinetics of these biochemical processes with the dynamics of motility may help us better understand social behaviour of bacteria.

Received 8 August 2011.

References

1. Alben, S. & Shelley, M. 2005 Coherent locomotion as an attracting state for a free flapping body. *Proc. Natl. Acad. Sci. U.S.A*. 102, 11163–11166.
2. Anderson, J. 1989 Colloid transport by interfacial forces. *Ann. Rev. Fluid Mech*. 21, 61–99.
3. Batchelor, G. 1970 Slender body theory for particles of arbitrary cross-section in stokes flow. *J. Fluid Mech*. 44, 419–440.
4. Batchelor, G. 1977 The effect of brownian motion on the bulk stress in a suspension of spherical particles. *J. Fluid Mech*. 83, 97–117.
5. Batchelor, G. & Green, J. 1972 The determination of the bulk stress in a suspension of spherical particles to order c^2. *J. Fluid Mech*. 56, 401–427.
6. Batchelor, G. K. & Green, J. T. 1972 The hydrodynamic interaction of two small freely-moving spheres in a linear flow field. *J. Fluid Mech*. 56, 375–400.
7. Becker, L., Koehler, S. & Stone, H. 2003 On self-propulsion of micro-machines at low reynolds number: Purcell's three-link swimmer. *J. Fluid Mech*. 490, 15–35.
8. Bees, M. & Hill, N. 1997 Wavelengths of bioconvection patterns. *J. Exp. Biol*. 200, 1515–1526.
9. Bees, M. & Hill, N. 1998 Linear bioconvection in a suspension of randomly swimming gyrotactic microorganisms. *Phys. Fluids* 10(8), 1864–1881.
10. Bees, M. & Hill, N. 1999 Non -linear bioconvection in a deep suspension of gyrotactic swimming microorganisms. *J. Math. Biol*. 38, 135–168.
11. Berg, H. 1983 *Random walks in biology*. Princeton, New Jersey: Princeton University Press.
12. Berg, H. 2000 Motile behavior of bacteria. *Phys. Today* 53, 24–29.
13. Berg, H. 2009 The gain paradox. *Prog. Biophys. Mol. Biol*. 100(1–3), 2–3.
14. Berke, A., Turner, L., Berg, H. & Lauga, E. 2008 Hydrodynamic attraction of swimming microorganisms by surfaces. *Phys. Rev. Lett*. 101, 038102.
15. Bertin, E., Droz, M. & Gregoire, G. 2006 Boltzmann and hydrodynamic description for self-propelled particles. *Phys. Rev. E* 74, 022101.
16. Betterton, M. & Brenner, M. 2001 Collapsing bacterial cylinders. *Phys. Rev. E* 64, 061904.
17. Blake, J. 1971 Infinite models for ciliary propulsion. *J. Fluid Mech*. 49, 209–222.
18. Blake, J. 1973 A finite model for ciliated micro-organisms. *J. Biomech*. 6(2), 133–140.
19. Block, S., Segall, J. & Berg, H. 1983 Adaptation kinetics in bacterial chemotaxis. *J. Bacteriol*. 154(1), 312–323.
20. Brady, J. & Bossis, G. 1985 The rheology of concentrated suspensions of spheres in simple shear flow by numerical simulation. *J. Fluid Mech*. 155, 105–129.
21. Brady, J. & Morris, J. 1997 Microstructure of strongly sheared suspensions and its impact on rheology and diffusion. *J. Fluid Mech*. 348, 103–139.
22. Brady, J. F. & Bossis, G. 1988 Stokesian dynamics. *Ann. Rev. Fluid Mech*. 20, 111.

23. Brennen, C. 1974 An oscillating boundary-layer theory for ciliary propulsion. *J. Fluid Mech*. 65, 799–824.
24. Brennen, C. & Winet, H. 1977 Fluid mechanics of propulsion by cilia and flagella. *Ann. Rev. Fluid Mech*. 9, 339–398.
25. Brenner, H. 1974 Rheology of a dilute suspension of axisymmetric brownian particles. *Int. J. Multiphase Flow* 1(2), 195–341.
26. Brenner, M., Levitov, L. & Budrene, E. 1998 Physical mechanisms for chemotactic pattern formation by bacteria. *Biophys. J*. 74, 1677–1693.
27. Brown, D. & Berg, H. 1974 Temporal stimulation of chemotaxis in *escherichia coli*. *Proc. Nat. Acad. Sci*. 71, 1388–1392.
28. Chaikin, P. & Lubensky, T. 2000 *Principles of condensed matter physics*. Cambridge, United Kingdom: Cambridge University Press.
29. Chapman, S. & Cowling, T. 1991 *The mathematical theory of non-uniform gases*. Cambridge, United Kingdom: Cambridge University Press.
30. Childress, S. 1981 *Mechanics of swimming and flying*. Cambridge: Cambridge University Press.
31. Childress, S. & Dudley, R. 2004 Symmetry breaking leads to forward flapping flight. *J. Fluid Mech*. 506, 147–155.
32. Childress, S. & Dudley, R. 2004 Transition from ciliary to flapping mode in a swimming mollusc: Flapping flight as a bifurcation in re_{ω}. *J. Fluid Mech*. 498, 257–288.
33. Childress, S., Levandowsky, M. & Spiegel, E. 1975 Pattern formation in a suspension of swimming microorganisms: equations and stability theory. *J. Fluid Mech*. 63, 591–613.
34. Clements, K. & Bullivant, S. 1991 An unusual symbiont from the gut of surgeonfishes may be the largest known prokaryote. *J. Bacteriol*. 173, 5359–5362.
35. Cox, R. 1970 The motion of long slender bodies in a viscous fluid part 1. general theory. *J. Fluid Mech*. 44, 791–810.
36. Crenshaw, H. 1993 Orientation by helical motion—ii. changing the direction of the axis of motion. *Bull. Math. Biol.* 55(1), 213–230.
37. Crenshaw, H. 1996 A new look at locomotion in microorganisms: rotating and translating. *Amer. Zool*. 36(6), 608–618.
38. Dombrowski, C., Cisneros, L., Chatkaew, S., Goldstein, R. & Kessler, J. 2004 Self-concentration and large-scale coherence in bacterial dynamics. *Phys. Rev. Lett*. 93, 098103.
39. Drazin, P. G. & Reid, W. H. 2004 Hydrodynamic stability. Cambridge: Cambridge University Press
40. Drescher, K., Goldstein, R., Michel, N., Polin, M. & Tuval, I. 2010 Direct measurement of the flow field around swimming microorganisms. *Phys. Rev. Lett*. 105, 168101.
41. Dreyfus, R., Baudry, J., Roper, M., M. Fermigier, H. S. & Bibette, J. 2005 Microscopic artificial swimmers. *Nature* 437, 862–865.
42. Eames, I., Gobby, D. & Dalziel, S. 2003 Fluid displacement by stokes flow past a spherical droplet. *J. Fluid Mech*. 485, 67–85.
43. Felderhof, B. 2006 The swimming of animalcules. *Phys. Fluids* 18, 063101–1–063101–9.
44. Fenchel, T. 1994 Motility and chemosensory behaviour of the sulphur bacterium *thiovulum majus*. *Microbiol.* 140(11), 3109–3116.
45. Ghorai, S. & Hill, N. 1999 Development and stability of gyrotactic plumes in bioconvection. *J. Fluid Mech*. 400, 1–31.
46. Ghorai, S. & Hill, N. 2000 Periodic arrays of gyrotactic plumes in bioconvection. *Phys. Fluids* 12(1), 5–22.
47. Ghorai, S. & Hill, N. 2007 Gyrotactic bioconvection in three dimensions. *Phys. Fluids* 19, 054107.
48. Goldstein, R., Goreily, A., Huber, G. & Wolgemuth, C. 2000 Bistable helices. *Phys. Rev. Lett*. 84(7), 1631–1634.
49. Golestanian, R. & Ajdari, A. 2008 Analytic results for the three-sphere swimmer at low reynolds number. *Phys. Rev. E* 77, 036308.
50. Gregoire, G. & Chate, H. 2004 Onset of collective and cohesive motion. *Phys. Rev. Lett*. 92, 025702.
51. Hernandez-Ortiz, J., Underhill, P. & Graham, M. 2009 Dynamics of confined suspensions of swimming particles. *J. Phys. Cond. Mat*. 21(20), 204107.
52. Hernandez-Ortiz, J. P., Stoltz, C. G. & Graham, M. D. 2005 Transport and collective dynamics in suspension of confined swimming particles. *Phys. Rev. Lett*. 95, 204501.
53. Hill, N. & Bees, M. 2002 Taylor dispersion of gyrotactic swimming microorganisms in a linear flow. *Phys. Fluids* 14(8), 2598–2605.
54. Hill, N., Pedley, T. & Kessler, J. 1989 Growth of bioconvection patterns in a suspension of gyrotactic microorganisms in a layer of finite depth. *J. Fluid Mech*. 208, 509–543.
55. Hillesdon, A. & Pedley, T. 1995 The development of concentration gradients in a suspension of chemotactic bacteria. *Bull. Math. Biol*. 57(2), 299–344.
56. Hillesdon, A. & Pedley, T. 1996 Bioconvection in suspensions of oxytactic bacteria: linear theory. *J. Fluid Mech*. 324, 223–259.
57. Hillesdon, A., Pedley, T. & Kessler, J. 1995 The development of concentration gradients in a suspension of chemotactic bacteria. *Bull. Math. Biol*. 57(2), 299–344.
58. Hinch, E. 1977 An averaged-equation approach to particle interactions in a fluid suspension. *J. Fluid Mech*. 83, 695–720.
59. Ishikawa, T. & Hota, M. 2006 Interaction of two swimming *paramoecia*. *J. Exp. Biol*. 209, 4452–4463.
60. Ishikawa, T. & Pedley, T. 2007 Diffusion of swimming model micro-organisms in a semi-dilute suspension. *J. Fluid Mech*. 588, 437–462.
61. Ishikawa, T. & Pedley, T. 2007 The rheology of a semi-dilute suspension of swimming model micro-organisms. *J. Fluid Mech*. 588, 399–435.
62. Ishikawa, T. & Pedley, T. 2008 Coherent structures in monolayers of swimming particles. *Phys. Rev. Lett*. 100(8), 088103.
63. Ishikawa, T., Simmonds, M. P. & Pedley, T. J. 2006 Hydrodynamic interaction of two swimming model micro-organisms. *J. Fluid Mech*. 568, 119–160.
64. J.E. Avron, O. K. & Oaknin, D. 2005 Pushmepullyou: an efficient micro-swimmer. *New J. Phys.* 7, 234.
65. Jeffery, G. 1922 The motion of ellipsoidal particles immersed in a viscous fluid. *Proc. Roy. Soc. Lond. A* 102, 161–179.
66. Keaveny, E. & Maxey, M. 2008 Spiral swimming of an artificial micro-swimmer. *J. Fluid Mech*. 598, 293–319.
67. Keller, E. & Segel, L. 1971 Model for chemotaxis. *J. Theor. Biol*. 30, 225–234.
68. Kessler, J. 1985 Hydrodynamic focusing of motile algal cells. *Nature* 313, 218–220.
69. Kessler, J. 1986 Individual and collective fluid dynamics of swimming cells. *J. Fluid Mech*. 173, 291–205.
70. Kessler, J. O. 1986 Individual and collective dynamics of swimming cells. *J. Fluid Mech*. 173, 191–205.
71. Kim, M., Bird, J., Park, J., Powers, T. & Breuer, K. 200r Particle image velocimetry experiments on a macro-scale model for bacterial flagellar bundling. *Exp. Fluids* 37(6), 782–788.
72. Kim, S. & Karrila, S. J. 2005 *Microhydrodynamics: Principles and Selected Publications*. Singapore: Dover.

73. Koiller, J., Ehlers, K. & Montgomery, R. 1996 Problems and progress in microswim-ming. *J. Nonlinear Sci.* 6, 507–541.
74. Ladd, A. 1994 Numerical simulations of particulate suspensions via a discretized boltzmann equation. part 1. theoretical foundation. *J. Fluid Mech*. 271, 285–309.
75. Lauga, E. 2007 Continuous breakdown of purcell's scallop theorem with inertia. *Phys. Fluids* 19, 061703–1–061703–4.
76. Lauga, E. 2008 No many-scallop theorem: Collective locomotion of reciprocal swimmers. *Phys. Rev. E* 78, 030901–1–030901–4.
77. Lauga, E. 2009 Life at high deborah number. *Eur. Phys. Lett*. 86, 64001–1–64001–6.
78. Lauga, E. & Powers, T. 2009 The hydrodynamics of swimming microorganisms. *Rep. Prog. Phys*. 72(9), 096601.
79. L.E. Becker, S. K. & Stone, H. 2003 On self-propulsion of micro-machines at low reynolds number: Purcell's three-link swimmer. *J. Fluid Mech*. 490, 15–35.
80. Leal, L. 2007 *Advanced transport phenomena: fluid mechanics and convective transport processes*. New York: Cambridge series in chemical engineering.
81. Leoni, M., Kotar, J., Bassetti, B., Cicuta, P. & Lagomarsino, C. 2003 A basic swimmer at low reynolds number. *Soft Matter* 5, 472–476.
82. Lighthill, J. 1976 Flagellar hyrodynamics. *SIAM Rev*. 18, 161–230.
83. Lighthill, M. J. 1952 On the squirming motion of nearly spherical deformable bodies through liquids at very small Reynolds numbers. *Comm. Pure Appl. Math*. 5, 109–118.
84. Lighthill, M. J. 1969 Hydromechanics of aquatic animal propulsion. *Ann. Rev. Fluid Mech*. 1, 413–446.
85. Llopis, I. & Pagonabarraga, I. 2006 Dynamic regimes of hydrodynamically coupled self-propelling particles. *Europhys. Lett*. 75, 999–1005.
86. Lu, X. & Liao, Q. 2006 Dynamic responses of a two-dimensional flapping foil motion. *Phys. Fluids* 18, 098104–1–098104–4.
87. Magar, V., Goto, T. & Pedley, T. 2003 Nutrient uptake by a self-propelled steady squirmer. *Quat. J. Mech. Appl. Math*. 56(1), 65–91.
88. Manela, A. & Frankel, I. 2003 Generalized taylor dispersion in suspensions of gyrotactic swimming microorganisms. *J. Fluid Mech*. 490, 99–127.
89. Manson, M., Armitage, J., Hoch, J. & Macnab, R. 1998 Bacterial locomotion and signal transduction. *J. Bacteriol*. 180(5), 1009–1022.
90. Mehandia, V. & Nott, P. R. 2008 The collective dynamics of self-propelled particles. *J. Fluid Mech*. 595, 239–264.
91. Najafi, A. & Golestanian, R. 2004 Simple swimmer at low reynolds number: Three linked spheres. *Phys. Rev. E* 69, 062901–1–063101–4.
92. Nott, P. & Brady, J. 1994 Pressure-driven flow of suspensions: Simulation and theory. *J. Fluid Mech*. 275, 157–199.
93. Pedley, T., Hill, N. & Kessler, J. 1988 The growth of bioconvection patterns in a uniform suspension of gyrotactic microorganisms. *J. Fluid Mech*. 195, 223–237.
94. Pedley, T. & Kessler, J. 1990 A new continuum model for suspensions of gyrotactic microorganisms. *J. Fluid Mech*. 212, 155–182.
95. Pedley, T. & Kessler, J. 1992 Hydrodynamic phenomena in suspensions of swimming microorganisms. *Ann. Rev. Fluid Mech*. 24, 313–358.
96. Pine, D., Gollub, J., Brady, J. & Leshansky, A. 2005 Chaos and threshold for irreversibility in sheared suspensions. *Nature* 438, 997–1000.
97. Platt, J. R. 1961 Bioconvection patterns in cultures of free-swimming organisms. Science, 133, 1766-1767.
98. Polin, M., Tuval, I., Drescher, K., Gollub, J. & Goldstein, R. 2009 Chlamy-domonas swims with two "gears" in a eukaryotic version of run-and-tumble locomotion. *Science* 325, 487–490.
99. Pooley, C. & Yeomans, J. 2007 Hydrodynamic interaction between two swimmers at low reynolds number. *Phys. Rev. Lett*. 99, 228103.
100. Purcell, E. M. 1977 Life at low Reynolds number. *Americal J. of Physics* 45 (1), 3–11.
101. Rafai, S., Jibuti, L. & Peyla, P. 2010 E3ective viscosity of microswimmer suspensions. *Phys. Rev. Lett*. 104, 098102.
102. Ramachandran, S., Sunil Kumar, P. B. & Pagonabarraga, I. 2006 A lattice-Boltzmann model for suspensions of self-propelling colloidal particles. *Eur. Phys. J. E* 20, 151–158.
103. Ramaswamy, S. & Rao, M. 2007 Active-filament hydrodynamics: instabilities, boundary conditions and rheology. *New J. Phys*. 9, 423.
104. Reddy, M. 2011 Collective dynamics of swimming microorganisms. *ME report, Indian Institute of Science* .
105. R.M., M. 1977 Bacterial flagella rotating in bundles: a study in helical geometry. *Proc. Nat. Acad. Sci*. 74(1), 221–1–225.
106. Rothschild, L. 1963 Non-random distribution of bull spermatozoa in a drop of sperm suspension. *Nature* 198, 1221–1222.
107. Russel, W., Saville, D. & Schowalter, W. 1989 *Colloidal dispersions*. Cambridge: Cambridge University Press.
108. Saintillan, D. & Shelley, M. 2007 Orientational order and instabilities in suspensions of locomoting rods. *Phys. Rev. Lett*. 99, 058102.
109. Segall, J., Block, S. & Berg, H. 1986 Temporal comparisons in bacterial chemotaxis. *Proc. Nat. Acad. Sci*. 83, 8987–8991.
110. Shapere, A. & Wilczek, F. 1989 Geometry of self-propulsion at low reynolds number. *J. Fluid Mech*. 198, 557–1–585.
111. Sierou, A. & Brady, J. F. 2001 Accelerated Stokesian dynamics. *J. Fluid Mech*. 448, 115–146.
112. Simha, R. A. & Ramaswamy, S. 2002 Hydrodynamic fluctuations and instabilities in ordered suspensions of self-propelled particles. *Phys. Rev. Lett*. 89 (5), 58101.
113. Sokolov, A. & Aranson, I. 2009 Reduction of viscosity in suspension of swimming bacteria. *Phys. Rev. Lett*. 103, 148101.
114. Subramanian, G. 2010 Viscosity-enhanced biomixing of the oceans. *Curr. Sci*. 98(8), 1103–1108.
115. Subramanian, G. & Koch, D. 2009 Critical bacterial concentration for the onset of collective swimming. *J. Fluid Mech*. 632, 359–400.
116. Subramanian, G., Koch, D. & Fitzgibbon, S. 2011 The stability of a homogeneous suspension of chemotactic bacteria. *Phys. Fluids* 23, 041901.
117. Tam, D. & Hosoi, A. 2007 Optimal stroke patterns for purcell's three-link swimmer. *Phys. Rev. Lett*. 98, 068105–1–068105–4.
118. Taylor, G. I. 1951 Analysis of the swimming of microscopic organisms. *Proc. Roy. Soc. A* 209, 447.
119. Thar, R. & Fenchel, T. 2001 True chemotaxis in oxygen gradients of the sulfur-oxidizing bacterium *thiovulum majus*. *Appl. Environ. Microbiol*. 67, 3299–3303.
120. Thar, R. & Kuhl, M. 2003 Bacteria are not too small for spatial sensing of chemical gradients: an experimental evidence. *Proc. Nat. Acad. Sci*. 100(10), 5748–5753.
121. Toner, J. & Tu, Y. 1995 Long-range order in a two-dimensional dynamical xy mode: how birds fly together. *Phys. Rev. Lett*. 75, 4326–4329.

122. Toner, J. & Tu, Y. 1998 Flocks, herds and schools: A quantitative theory of flocking. *Phys. Rev. E* 58, 4828–4858.
123. Tu, Y., Shimizu, T. & Berg, H. 2008 Modeling the chemotactic response of *escherichia coli* to time-varying stimuli. *Proc. Nat. Acad. Sci*. 105, 14855–14860.
124. Tuck, E. 1968 A note on a swimming problem. *J. Fluid Mech*. 31, 305–308.
125. Underhill, P., Hernandez-Ortiz, J. & Graham, M. 2008 Diffusion and spatial correlations in suspensions of swimming particles. *Phys. Rev. Lett*. 100, 248101.
126. Vicsek, T., Czirok, A., Ben-Jacob, E., Cohen, I. & Shochet, O. 1995 Novel type of phase transition in a system of self-driven particles. *Phys. Rev. Lett*. 75 (6), 1226.
127. Vincent, R. & Hill, N. 1996 Bioconvection in a suspension of phototactic algae. *J. Fluid Mech*. 327, 343–371.
128. Vuppula, R., Tirumkudulu, M. & Venkatesh, K. 2010 Chemotaxis of *escherichia coli* to *l*-serine. *Phys. Biol*. 7, 026007.
129. Wager, H. 1911 On the effect of gravity upon the movements and aggregation of euglena viridis, ehrb., and other microorganisms. *Proc. Phil. Trans. Royal Soc. London, B* 201, 333–390.
130. Wiggins, C. & Goldstein, R. 1998 Flexive and propulsive dynamics of elastica at low reynolds number. *Phys. Rev. Lett*. 80(17), 3879–3882.
131. Williams, C. & Bees, M. 2011 Photo-gyrotactic bioconvection. *J. Fluid Mech*. 678, 41–86.
132. Wu, M., Roberts, J., Kim, S., Koch, D. & DeLisa, M. 2006 Collective bacterial dynamics revealed using a three-dimensional population-scale defocused particle tracking technique. *Appl. Env. Microbiol*. 72(7), 4987–4994.
133. Wu, X. & Libchaber, A. 2000 Particle diffusion in a quasi-two-dimensional bacterial bath. *Phys. Rev. Lett*. 84, 3017–3020.
134. It is important to note that the principle of reversibility is a dynamic one; one that applies to the equations of motion. The kinematic relations, $dx/dt = \mathrm{u}(\mathrm{x}, t)$, that determine the actual particle pathlines are usually strongly non-linear. Thus, although the Stokes equations continue to be reversible in principle, one would never observe the exact reversal of a trajectory, over any significant time interval, in practice, owing to the extreme sensitivity to perturbations from the theoretical reversible trajectory[95].
135. The bacteria *Listeria* and *Shigella*, for example, propel themselves by growing a polymerized actin tail.
136. *E. fisheloni*, one of world's largest prokaryotes grows to sizes exceeding 0.5 *mm*(!), and swims by way of a mat of flagella that structurally resemble the prototypical bacterial flagellum, with diameters of 14–18 *nm*, and that cover the entire surface of the bacterium just like in the case of eukaryotic ciliates[34].
137. The transport of proteins occurs through this hollow centre.
138. The onset of the bundling process may be purely kinematic. As the cell starts swimming due to a momentary anisotropy in the flagella orientations, the drag due to this swimming motion will act to sweep the flagella to the rear, amplifying the initial small anisotropy. The argument may be reversed to argue why the cell may not translate over any significant distance when the flagella rotate in a clockwise manner. This would seem to account for the erratic motion during a tumble; although, the actual scenario is complicated by the polymorphic transformations of the individual flagella accompanying motor reversal[47, 103].
139. Recent experiments on *Chlamydomonas reinhardtii*, swimming in the dark, have shown that the algae executes a eukaryotic version of the run-and-tumble dynamics known to characterize the motion of peritrichously flagellated bacteria. Such a motion results from the intermittent switching of the anterior flagella between synchronous and asynochronous modes. The former mode, in which the flagella beat in unison, leads to a sustained (helical) motion along a given direction, while the latter mode, which is characterized by a large inter-flagella frequency difference, leads to a sharp change in the swimming direction[96].
140. Some of the larger bacteria (an example is *Thiovulum majus*[43,117]) exhibit a steering mechanism similar to eukaryotes. Interestingly, there are also instances of smaller prokaryotes having evolved a spatial sensing mechanism[118].
141. Hydrodynamic focussing of algal cells, arising from lateral gyrotactic migration, may also be achieved using an imposed shear flow rather than one driven by buoyancy[67]; one that may be exploited to separate cells based on motility and swimming behavior.
142. The phase transition predicted in the two-dimensional equilibrium setting is one of an infinite order, the Kosterlitz-Thouless transition, wherein the high-temperature disordered phase with exponentially decaying correlation functions gives way to one that exhibits only a quasi long-range order characterized by algebraically decaying correlation functions.
143. Here, we have made the restriction to slender-bodied swimmers, in which case the force-dipole is, at leading order, given by the axial moment of the linear force density.
144. Pair-interactions in a disordered system are usually expected to play a role only at $(nL^3)^2$).
145. This may also be seen from the criterion (14), wherein D_r must now be given by the result of a pair-interaction calculation.
146. The introduction of a rotary diffusivity is expected to render the spectrum purely discrete. This is similar to the effect of a finite viscosity in classical hydrodynamic stability—the Rayleigh equation, that governs the stability of inviscid perturbations in shearing flows, usually support a continuous spectrum, while the Orr-Sommerfeld equation has a purely discrete spectrum (for bounded domains). A more precise analogy may be drawn between the evolution of the orientation field in a bacterium suspension and the evolving vorticity field in a sheared inviscid fluid.
147. The original simulations of [51] showed an apparent upturn in the swimmer diffusivity beyond a critical concentration; however, this has been shown to an artifact of using point-force hydrodynamics without regularization[50].
148. The absence of short-ranged lubrication interactions would mean that the slender swimmers, to the order examined, are allowed to pass 'through' one another.
149. From symmetry considerations, it is easy to see that a force dipole at the geometric centre does not yield propulsion.

Ganesh Subramanian obtained his B.Tech. degree in 1996 from ICT-Mumbai, and a Ph.D. in chemical engineering, in 2002, from the California Institute of technology, Pasadena, CA, USA. He was a post-doctoral scholar in the department of chemical and bio-molecular engineering, Cornell University, NY, USA, from August 2002 to June 2005. He joined the Engineering mechanics Unit at the Jawaharlal Nehru center for advanced scientific research (JNCASR) as a Faculty Fellow in November 2005, and was promoted to Associate Professor in May 2011.
Ganesh Subramanian's research interests include the dynamics and rheology of complex fluids, vortex dynamics and stability, and the role of radiation in the dynamics of the nocturnal boundary layer. He has been a Young Associate of the Indian Academy of Sciences, and was a recipient of the Young Engineer Award (2010) instituted by the Indian National Academy of Engineering.

Prabhu Nott obtained his bachelor's degree from IIT Madras, and his doctoral degree from Princeton University, both in chemical engineering. He has been in the faculty of the Chemical Engineering department at the Indian Institute of Science since 1993. His research interests are on the flow of granular materials, particle-fluid suspensions, and the dynamics of interacting microorganisms.